Mathematical modelling of impurity deposition during evaporation of dirty liquid in a porous material

Ellen K. Luckins[1]†, Christopher J. W. Breward[2], Ian M. Griffiths[2] and Colin P. Please[2]

[1]Mathematics Institute, Zeeman Building, University of Warwick, Coventry CV4 7AL, UK

[2]Mathematical Institute, University of Oxford, Andrew Wiles Building, Woodstock Road, Oxford OX2 6GG, UK

(Received xx; revised xx; accepted xx)

When a contaminated liquid evaporates from within a porous material (PM), the impurities or dirt accumulate and deposit within the porespace. This occurs during the cleaning of filters and fouling of textiles, and is related to the "coffee-ring" problem. To investigate how and where dirt is deposited in the porespace, we present a model for the motion of an evaporation front through a PM, and the related accumulation, transport, and deposition of dirt, assuming that the liquid remains stationary. For physically relevant parameters, vapour transport out of the PM is quasi-steady and we derive a single ordinary differential equation describing the motion of the evaporation front in time. Model solutions exhibit spatially non-uniform profiles of the deposited-dirt layer thickness through the PM. The dirt accumulation and evaporation problems are coupled: deposited dirt hinders vapour transport through the PM, slowing the evaporation. We identify two scenarios in which the PM becomes clogged with dirt. Accumulation of suspended dirt at the evaporating interface along with slow dirt diffusion results in the deposited-dirt layers clogging the pores at the evaporating interface, halting the drying and trapping liquid in the PM. Alternatively, slow dirt-deposition results in the suspended dirt being pushed far into the PM by the evaporation, eventually leaving only dirt (with no liquid) in the porespace. We investigate the dynamics of both clogging scenarios, characterising the parameter regimes for which each occurs. Both clogging scenarios must be avoided in practice since they may be detrimental to future filter efficacy or textile breathability.

Key words: Authors should not enter keywords on the manuscript

1. Introduction

Drying-driven redistribution of dirt within filters and textiles is a common problem, with practical industrial importance. For instance, after the rinsing of filters used in vacuum

† Email address for correspondence: ellen.luckins@warwick.ac.uk

cleaners or washing machines, the filter dries and any remaining dirt or cloth fibres are left in the filter (Ji & Sanaei 2023), reducing its capacity for the next filtration cycle. Waterproof clothing such as coats and boots will dry after use, and impurities or dirt may similarly be left within the pores of the textile and waterproof membrane (Breward *et al.* 2020; Sanaei *et al.* 2022).

A key question in these filtration and waterproof-clothing applications is to determine where within the porous material the dirt is deposited once the liquid has all evaporated. We might also ask whether all of the liquid can indeed be evaporated, or whether it becomes trapped in regions of porespace clogged by the deposited dirt. In the applications of interest, it is important that the dirt does not clog the material, as this leads to reduced filter efficacy, or reduced breathability of the waterproof garment. Furthermore, trapped water in a washing machine filter may contribute to the growth of bacteria or mould, and should be avoided for hygiene reasons (Abney *et al.* 2021). A paradigm situation encompassing these processes is that of a porous material containing a mixture of a liquid, such as water, and an impurity or dirt that is suspended in the liquid. As the liquid evaporates, an evaporation front moves into the porous material from its surface. The dirt is left behind in the liquid as the liquid evaporates, and may deposit into a layer on the walls of the porespace.

A related problem is the deposition of suspended particles when a droplet of liquid dries on an impermeable substrate. This is known to lead to a coffee-ring effect, in which the coffee particles are transported by evaporation-induced flow of liquid to the edge of the droplet. This coffee-ring effect is well studied, for instance by Deegan *et al.* (1997, 2000); Karapetsas *et al.* (2016); Kaplan & Mahadevan (2015); Moore *et al.* (2021); Murisic & Kondic (2011); Popov (2005), and recently reviewed by Wilson & D'Ambrosio (2023). The coffee-ring effect is of practical importance, for instance in the drying of ink droplets in ink-jet printing (Mampallil & Eral 2018; Soltman & Subramanian 2008) and in the manufacture of electronic devices (D'Ambrosio *et al.* 2021).

In a drying porous material, such as a filter membrane or textile, there are several additional complications not present in the coffee-ring set-up. Firstly, the problem is multiscale in nature, in that the fluid flow, evaporation, and the transport and deposition of the dirt occur within the pore-space, while the depth of porous material to be dried is likely to be significantly larger than an individual pore, even for fairly thin filter membranes. It is not immediately clear how to formulate a model that captures the porescale behaviour and yet remains tractable over the scale of the entire drying material. Additionally, dirt deposition may occur throughout the porous domain, not only at the base of the evaporating droplet. This means that there is additional coupling between the drying and the deposition: like in evaporating droplets, the accumulation of suspended dirt at the evaporating interface can reduce the evaporation rate (Karapetsas *et al.* 2016), but additionally the build-up of deposited dirt in the porespace affects the porosity and reduces the rate of diffusive transport of (i) the suspended dirt through the liquid-saturated porespace, and (ii) vapour out through the dry porous material. In extreme cases, the deposited dirt might completely clog the pore-space at the evaporation front, terminating the drying before all liquid is evaporated. This phenomenon is not possible in coffee-ring problems. Like the surface-tension driven flows in coffee-rings, a capillary flow may draw fluid through the porous material, which then evaporates near the surface of the porous material (Lehmann *et al.* 2008). This is typically the case early in the drying process ("Stage I"), while later ("Stage II") the evaporating interface moves into the porous material, and the transport of vapour out of the porous material limits the evaporation rate (Fei *et al.* 2022; Or *et al.* 2013).

Drying porous media (without dirt) have been studied in a variety of settings and using various different modelling techniques. Depending on the porous material and fluids, various drying regimes are possible: liquid and gas may co-exist within the porespace throughout

the entire medium and for the majority of the drying time (so that the majority of the drying is in Stage I), or a region in which capillary effects dominate, often referred to as a"film region", may separate a region of porous material saturated with liquid from a multi-phase region incorporating unconnected pockets of stationary liquid (Lehmann *et al.* 2008; Pel *et al.* 2002). Multi-phase flow models for drying are derived by, for instance, Whitaker (1977) while lumped models, consisting of nonlinear diffusion equations for the "moisture" (combining liquid and vapour) are also often used (Pel *et al.* 2002; Vu & Tsotsas 2018). Evaporation within the pore-space may be simulated directly, although this is computationally expensive and limited to sufficiently small domain sizes (Fei *et al.* 2022). Pore-network models are a more computationally tractable approximation, although the details of the fluid flow are neglected (Nowicki *et al.* 1992; Tsimpanogiannis *et al.* 1999).

The transport and trapping of particles in a liquid-saturated porous material when the liquid is flowing is known as deep-bed filtration (Zamani & Maini 2009). When there is no flow of the liquid, the particles may still be transported by Brownian diffusion (Epstein 1988). Particles may build up in a deposited layer on the pore walls due to several mechanisms, including electrostatic forces in the bulk (Zamani & Maini 2009). Particles are generally repelled from air–water interfaces unless they are hydrophobic; in the hydrophobic case they might be held at the interface and thus transported more effectively with it (Flury & Aramrak 2017). Particles may deposit or attach to the walls of the pore-space due to adsorption, electrostatic forces, or other chemical binding mechanisms (Dressaire & Sauret 2017; Epstein 1988; Zamani & Maini 2009). Experimental work such as that of Gudipaty *et al.* (2011); Linkhorst *et al.* (2016); Stamm *et al.* (2011) seeks to visualise the deposits and quantify their growth rates in terms of the system parameters.

For an evaporating droplet, an evaporative flux is generally prescribed at the droplet surface (Kaplan & Mahadevan 2015; Karapetsas *et al.* 2016; Murisic & Kondic 2011; Moore *et al.* 2021; Popov 2005). This flux may be constant (Moore *et al.* 2021), but typically depends on the distance from the edge of the droplet, accounting for the quasi-steady transport of vapour away from the droplet (Karapetsas *et al.* 2016; Popov 2005). When drying from within porous media, a prescribed evaporation rate may be appropriate during Stage I (when the evaporation occurs near the surface of the material) but, since the Stage II drying of porous media is limited by the removal of vapour from the porespace (Lehmann *et al.* 2008), like the majority of evaporating drops (Wilson & D'Ambrosio 2023), we expect that the evaporation rate will depend on the position of the evaporating interface within the porous material during this stage.

The deposition of dirt during the drying of a filter has recently been studied by Ji & Sanaei (2023). Here, the suspended dirt is assumed to diffuse through a liquid-saturated region of porous material ahead of an evaporating interface, and deposit at a rate directly proportional to its concentration, causing the local porosity to decrease. The evaporating interface is assumed to move through the porous material at a prescribed speed, dependent only on the local porosity and suspended dirt concentration, and not the location of the front within the filter. Simulations of this model show that the porosity of the filter decreases during the drying, and that the deposited dirt is non-uniformly distributed in the porespace once the drying is complete.

In this paper, we will systematically derive a homogenised model for the coupled processes of evaporation, transport of liquid vapour, diffusion and deposition of dirt in a drying porous material, starting from a pore-scale model for these processes. This analysis is based on previous work (Luckins *et al.* 2023) for evaporation of a pure liquid in a porous material, extended to incorporate dirt transport and deposition. One benefit of the homogenisation approach is that the pore-scale behaviour is included in the homogenised model through averaged terms. This ensures that the model conserves mass of all species, and also results in

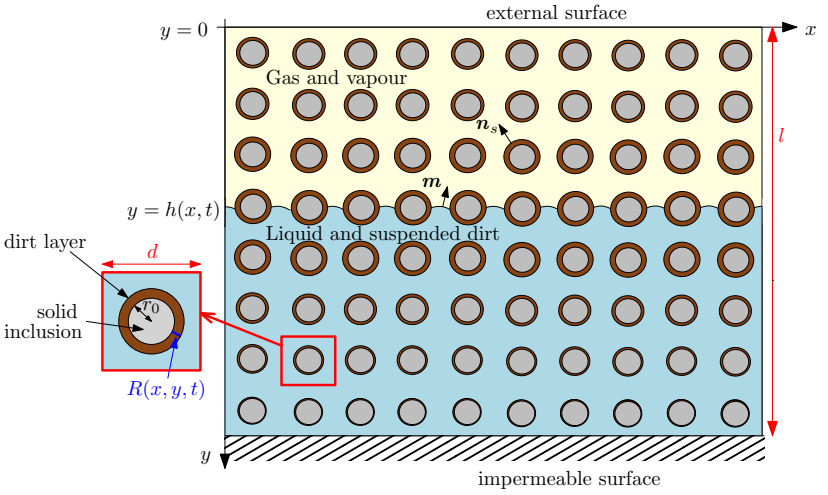

Figure 1: Schematic showing the evaporation front at $y = h(x,t)$ moving through the porespace (lengthscale d) of a porous material (of depth $l \gg d$), with dirt depositing in a layer of thickness $R(x,y,t)$ on the circular solid inclusions with radius r_0. The unit normal to the solid or dirt boundary of the porespace is $\boldsymbol{n}_s$, while the evaporating interface has unit normal $\boldsymbol{m}$.

a different diffusive term in the homogenised equations compared with the model posed by Ji & Sanaei (2023). For simplicity, as in both Luckins *et al.* (2023) and Ji & Sanaei (2023), we will assume that capillary flows are negligible and a sharp evaporating interface moves into the porous material. In practice, such systems would be valid when viscous or gravitational forces dominate over surface tension, for instance if the solid is hydrophobic (Shokri *et al.* 2008), or the pores are sufficiently large relative to the capillary lengthscale (Lehmann *et al.* 2008). Our coupled model for the drying and dirt transport is a type of Stefan problem, with undercooling in certain parameter regimes. We derive our homogenised model in section 2. In section 3 we note that the vapour transport is quasi-steady for physically relevant parameter choices and reduce the vapour-transport problem to a single ordinary differential equation (ODE) for the position of the evaporation front, providing a comparison between this model and that of Ji & Sanaei (2023). In section 4 we study the early-time behaviour of our model and describe our numerical solution method. In sections 5–6 we study the asymptotic limits of slow and fast deposition rates, identifying a distinct mechanism in each case by which the system may clog before the drying is complete. We quantify the parameter regimes for which these clogging phenomena occur in section 7 before concluding in section 8.

2. Model derivation

We consider a porous material of finite thickness l, initially with uniform porosity and saturated with a uniform mixture of liquid and suspended dirt. We assume that the dirt particles are small relative to the pore-lengthscale, and neither interact with each other nor dissolve in the liquid. The dirt–liquid mixture is thus a suspension of these insoluble dirt particles. We suppose the porous material is bounded by an impermeable solid material on one side. The liquid begins to evaporate from the side open to the atmosphere, leaving the dirt behind, and an evaporation front moves into the porous material, with the suspended dirt and liquid ahead of the front, and a mixture of inert gas (drawn in from above the porous material) and liquid vapour behind it. We assume the system is isothermal, with no variation

in temperature. A schematic of the situation under consideration is shown in figure 1. We consider a two-dimensional porous material for simplicity, with spatial variables x and y, and with y pointing *into* the porous material and $y = 0$ at the surface of the porous material. Although the structure of our model and the homogenisation analysis does not depend on the pore-scale geometry, it is helpful to specify this for simplicity. We choose a square lattice of circular solid inclusions, of radius r_0. We account for deposition of the suspended dirt onto the solid structure by considering deposited dirt layers of thickness $R(x, y, t)$, on each solid inclusion, which have initial thickness zero. An important assumption is that the liquid–dirt mixture does not flow, and so our model excludes any capillary pressure or surface tension effects (since in order to attain a (quasi-)static meniscus shape, the liquid would need to flow). We first consider the drying behaviour on the microscale — within the pores of the material — before averaging to derive our effective model. We suppose that the evaporating front is located at $y = h(x, t)$, splitting the domain into a region of porespace containing vapour in $0 \leqslant y \leqslant h(x, t)$, where the thickness of the layers of deposited dirt do not change with time, and a region of porespace in $h(x, t) \leqslant y \leqslant l$ containing the liquid–dirt mixture, where the dirt layer thicknesses vary in time due to deposition or erosion.

2.1. *Porescale model*

In the porespace occupied by vapour–gas mixture (behind the evaporating front, ie: $y < h(x, t)$), we expect the Reynolds number to be small (Luckins *et al.* 2023) and so we assume that the mixture satisfies the Stokes equations,

$$\nabla \cdot \boldsymbol{u} = 0, \qquad -\nabla p + \mu \nabla^2 \boldsymbol{u} = \boldsymbol{0}, \tag{2.1}$$

where $\boldsymbol{u}$ is the mass averaged velocity of the mixture, p is the pressure, and μ is the viscosity (assumed constant). The vapour contained within the mixture is advected with the flow, and also diffuses through the mixture with diffusivity D_v, and thus the density of the vapour, ρ_v [kg m^{-3}], satisfies

$$(\rho_v)_t + \boldsymbol{u} \cdot \nabla \rho_v = D_v \nabla^2 \rho_v, \tag{2.2}$$

where the subscript t denotes partial derivative. The overall density of the inert gas–vapour mixture, ρ_G, is given by

$$\rho_G = \rho_g + \rho_v. \tag{2.3}$$

Wherever the gas–vapour mixture meets the solid walls of the porespace we suppose there is no flux or slip of the gas–vapour mixture, and no flux vapour into the solid material, so that on the solid–liquid or dirt–liquid boundary, with normal $\boldsymbol{n}_s$,

$$\boldsymbol{u} = \boldsymbol{0}, \qquad (\rho_v \boldsymbol{u} - D_v \nabla \rho_v) \cdot \boldsymbol{n}_s = 0. \tag{2.4}$$

In the liquid–dirt mixture in $y > h(x, t)$, we assume that there is no net flow of the mixture, and the suspended dirt and liquid diffuse against one another in an ideal mixture, due to Brownian motion. The suspended dirt volume fraction, θ, therefore satisfies

$$\theta_t = D_d \nabla^2 \theta, \tag{2.5}$$

where D_d is the diffusivity of suspended dirt in liquid. As discussed in Luckins *et al.* (2023), the assumption that the liquid does not flow means that capillary effects are neglected from the model.

At the solid walls of the porespace, we suppose that the suspended dirt can deposit onto the solid microstructure, forming a layer which may also then be eroded away. We suppose that the deposited layer has a dirt volume fraction θ_* which is the packing volume fraction of the dirt particles. We expect this to be close to one, as only a small amount of liquid (volume

fraction $1-\theta_*$) is trapped within the deposited dirt layer. Conservation of dirt across the interface is given by

$$\theta V_n + D_d \nabla\theta \cdot \boldsymbol{n}_s = \theta_* V_n, \tag{2.6}$$

where V_n is the normal velocity of the depositing/eroding interface. We note that, in order that there is no flow generated at the depositing interface, we assume that the dirt and liquid have the same mass density, so that the total mixture density is the same on either side of the depositing/eroding interface, while the dirt and liquid fractions can jump (see, for instance, Geng *et al.* (2023)).

We suppose that the dirt is deposited at a rate dependent on the local suspended dirt volume fraction, while the erosion rate depends on the (constant) packing volume fraction θ_*. (If there was a flow of the fluid, we might extend this model and allow the erosion rate to depend on the local shear stress.) Thus we prescribe

$$V_n = k_+\theta - k_-\theta_*, \tag{2.7}$$

where the constants $k_\pm$ have units $\mathrm{m\,s^{-1}}$. This type of law-of-mass-action deposition rate, in which the deposition rate is linear in the quantity of suspended dirt, is common in the phenomenological bed-filtration literature (Dressaire & Sauret 2017; Zamani & Maini 2009), and is also used by Ji & Sanaei (2023) as a model for adsorption of particles onto the deposit layer.

At the evaporating interface $y = h(x,t)$, we suppose that the inert gas and the dirt do not pass through the interface, while liquid turns into vapour. We thus impose conservation of mass of each of the liquid/vapour, gas, and suspended dirt, namely

$$-\rho_l(1-\theta)V_m + \rho_d D_d \nabla\theta\cdot\boldsymbol{m} = \rho_v\left(\boldsymbol{u}\cdot\boldsymbol{m} - V_m\right) - D_v\nabla\rho_v\cdot\boldsymbol{m}, \tag{2.8a}$$

$$0 = \rho_g\left(\boldsymbol{u}\cdot\boldsymbol{m} - V_m\right) + D_v\nabla\rho_v\cdot\boldsymbol{m}, \tag{2.8b}$$

$$-\rho_d\theta V_m - \rho_d D_d\nabla\theta\cdot\boldsymbol{m} = 0, \tag{2.8c}$$

where ρ_l and ρ_d are the densities of pure liquid and dirt, respectively. Combining these, we derive the more helpful form

$$-\rho_L V_m = \rho_G\left(\boldsymbol{u}\cdot\boldsymbol{m} - V_m\right), \tag{2.9a}$$

$$-\rho_L V_m = \rho_v\left(\boldsymbol{u}\cdot\boldsymbol{m} - V_m\right) - D_v\nabla\rho_v\cdot\boldsymbol{m}, \tag{2.9b}$$

$$\theta V_m + D_d\nabla\theta\cdot\boldsymbol{m} = 0, \tag{2.9c}$$

interpretable as a condition on each of $\boldsymbol{u}\cdot\boldsymbol{m}$, ρ_v, and θ, respectively, where $\rho_L = \rho_l(1-\theta)+\rho_d\theta$ is the (assumed constant) liquid–dirt mixture density. The normal velocity of the interface and unit normal to the interface are given by

$$V_m = \frac{h_t}{\sqrt{1+h_x^2}}, \qquad \boldsymbol{m} = \frac{(h_x,-1)}{\sqrt{1+h_x^2}}, \tag{2.10}$$

where subscripts t and x denote partial derivatives. In addition to (2.9), we also impose a no-slip condition for the gas-mixture velocity

$$u + vh_x = 0 \qquad \text{on } y = h(x,t). \tag{2.11}$$

Finally, we must also incorporate a condition that describes the chemistry governing the evaporation. In Luckins *et al.* (2023) the effect of different chemistry conditions were considered, and these were shown to affect the form of macroscale boundary conditions derived through a homogenisation analysis. For simplicity, we assume that the liquid and vapour are in chemical equilibrium at the evaporating interface. The chemical potential on

the liquid side of the interface is dependent on the amount of liquid $(1-\theta)$ at the interface, while the chemical potential on the gas mixture side depends on the density of vapour, ρ_v, at the interface. In general, we may express this chemical equilibrium as

$$\rho_v = \rho^* f(\theta) \qquad \text{on } y = h(x,t) \tag{2.12}$$

where ρ^* is the (constant) saturation vapour density when $\theta = 0$ and there is no suspended dirt, and the function $f(\theta)$ captures the dirt-dependence of the saturation vapour density. (We note that therefore $f(0) = 1$.) The presence of particles at the interface are expected to hinder the vaporisation; in both Ji & Sanaei (2023); Karapetsas *et al.* (2016) the evaporative flux is modelled as decreasing with increased particles on the fluid surface. We keep $f(\theta)$ general as far as possible, and in section 5 we will investigate the effect of different functional dependencies $f(\theta)$ on the drying rate. However, in our numerical simulations we will use the simple linear form

$$f(\theta) = 1 - \theta, \tag{2.13}$$

to capture the effect of the dirt inhibiting vaporisation. We choose this form so that the saturation vapour density scales with the amount of liquid at the interface.

At the surface of the porous material, we impose a constant atmospheric vapour density and atmospheric pressure

$$\rho_v = \rho_a, \quad p = p_a, \qquad \text{on } y = 0. \tag{2.14}$$

Dirt cannot diffuse through the impermeable boundary and thus so impose that

$$\theta_y = 0, \text{ at } y = l. \tag{2.15}$$

This depth l is assumed to be much greater than the typical pore-lengthscale, so that there is separation between the pore- and macro-lengthscales.

2.2. *Nondimensionalisation*

We nondimensionalise the vapour/gas problem in a similar way to Luckins *et al.* (2023), making the rescalings

$$\boldsymbol{x} = d\hat{\boldsymbol{x}}, \quad h = d\hat{h}, \quad t = \frac{d^2}{\epsilon\delta D_v}\hat{t}, \quad \rho_v = \rho^*\hat{\rho}, \quad \boldsymbol{u} = \frac{D_v\nu\epsilon}{d}\hat{\boldsymbol{u}}, \quad p = p_a + \frac{\mu D_v \nu}{d^2}\hat{p}, \tag{2.16}$$

where

$$\delta = \frac{\rho^*}{\rho_L}, \quad \epsilon = \frac{d}{l}, \quad \nu = \frac{\rho^*}{\rho_G}, \tag{2.17}$$

are dimensionless parameters representing the ratio of vapour density to liquid density, the ratio of pore- to macro-lengthscales, and the ratio of vapour to gas densities, respectively. In particular we note we have chosen the timescale associated with the speed of the motion of the evaporating interfaces on the microscale, ie: the timescale over which sufficient vapour is removed by diffusion to empty the microscale porespace of liquid. Making these rescalings and dropping the hat notation, the dimensionless microscale model is, in $y < h(x,t)$

$$\epsilon\nabla\cdot\boldsymbol{u} = 0, \qquad \epsilon\nabla^2\boldsymbol{u} = \nabla p, \qquad \epsilon\left(\delta\rho_t + \nu\boldsymbol{u}\cdot\nabla\rho\right) = \nabla^2\rho, \tag{2.18a}$$

while in $y > h(x,t)$,

$$\epsilon\sigma\theta_t = \nabla^2\theta. \tag{2.18b}$$

At gas–solid interfaces in $y < h(x,t)$ (which are stationary),

$$\boldsymbol{u} = \boldsymbol{0}, \qquad \nabla\rho\cdot\boldsymbol{n}_s = 0, \tag{2.18c}$$

and at liquid–solid interfaces in $y > h(x,t)$ (which move with velocity V_n),

$$\nabla\theta \cdot \boldsymbol{n}_s = \epsilon\sigma\,(\theta_* - \theta)\,V_n, \qquad V_n = \epsilon\kappa\,(\theta - \beta)\,, \tag{2.18d}$$

while at the evaporating interfaces $y = h(x,t)$,

$$\boldsymbol{u}\cdot\boldsymbol{m} - \delta\nu^{-1}\frac{h_t}{\sqrt{1+h_x^2}} = -\frac{h_t}{\sqrt{1+h_x^2}}, \tag{2.18e}$$

$$\epsilon\rho\left(\nu\boldsymbol{u}\cdot\boldsymbol{m} - \delta\frac{h_t}{\sqrt{1+h_x^2}}\right) - \nabla\rho\cdot\boldsymbol{m} = -\epsilon\frac{h_t}{\sqrt{1+h_x^2}}, \tag{2.18f}$$

$$u + vh_x = 0, \tag{2.18g}$$

$$\epsilon\sigma\theta V_m + \nabla\theta\cdot\boldsymbol{m} = 0, \tag{2.18h}$$

$$\rho = f(\theta). \tag{2.18i}$$

At the surface of the porous material,

$$\rho = \alpha \qquad \text{at } y = 0, \tag{2.18j}$$

while at the impermeable surface (or centre of a symmetric porous material),

$$\theta_y = 0 \qquad \text{at } y = \epsilon^{-1}. \tag{2.18k}$$

Here we have introduced the additional dimensionless parameters

$$\sigma = \delta\frac{D_v}{D_d}, \quad \kappa = \frac{k_+ d}{\epsilon^2\delta D_v}, \quad \beta = \frac{k_-\theta_*}{k_+}, \quad \alpha = \frac{\rho_a}{\rho^*} \tag{2.19}$$

which appear in the dirt problem, representing the ratio of the suspended-dirt diffusion timescale to the timescale of the evaporation-front motion, the ratio of the dirt deposition rate to the evaporation rate, the ratio of the dirt erosion rate to deposition rate, and the ratio of the atmospheric vapour density to the maximum saturation vapour density, respectively.

The micro- to macro-lengthscale ratio ϵ (defined in (2.17)) is the small parameter we will take advantage of in order to homogenise (2.18). As in Luckins *et al.* (2023) we will take $\delta < 1$ and $\nu < 1$ to be order one parameters relative to ϵ for the homogenisation analysis. We note that $\delta \approx 10^{-3}$ for water, so will later consider the additional limit of $\delta \to 0$ (which is equivalent to taking this limit before performing the homogenisation analysis). We require $\alpha < 1$ but expect $\alpha \ll 1$ to be reasonable. Although the diffusion of vapour in air is generally much faster than the diffusion of any kind of molecule through a liquid, so that $D_v \gg D_d$, we note that since $\delta \approx 10^{-3} - 10^{-4}$ is small, σ is likely to be order one. For instance if we take $D_v \approx 2.5\times10^{-5}\,\mathrm{m^2\,s^{-1}}$ and $D_d \approx 10^{-9}\,\mathrm{m^2\,s^{-1}}$, (Cussler 2009) then with $\delta = 10^{-4}$ we find $\sigma \approx 2.5$. We will consider the distinguished limit of $\sigma = O(1)$ in this paper, but we note there is an alternative, slow-dirt-diffusion distinguished limit with $\sigma = O(\epsilon^{-1})$. We discuss this alternative case further in the appendix A.2, and briefly in section 2.3 below. In summary, all of σ, κ, β, and α are taken to be order one relative to ϵ to homogenise the model.

2.3. *Summary of the homogenised drying model*

The homogenisation analysis is described in appendix A. The result of this analysis is a macroscale model for the vapour density ρ, suspended dirt volume fraction θ, deposited dirt-layer thickness, R, and position, $Y = H(T)$ of the evaporation front, namely

$$\delta\phi\rho_T - (\nu - \delta)\phi|_H H_T\rho_Y = (\mathcal{D}\rho_Y)_Y\,, \tag{2.20a}$$

for $Y < H(T)$, and

$$\sigma\phi\theta_T = (\mathcal{D}\theta_Y)_Y - \sigma\kappa C(\theta_* - \theta)(\theta - \beta\chi_R), \tag{2.20b}$$

$$R_T = \kappa(\theta - \beta\chi_R). \tag{2.20c}$$

for $Y > H(T)$. At $Y = H(T)$,

$$\mathcal{D}\rho_Y = (1 - \nu\rho)\phi H_T, \tag{2.20d}$$

$$\rho = f(\theta), \tag{2.20e}$$

$$\sigma\phi H_T\theta + \mathcal{D}\theta_Y = 0, \tag{2.20f}$$

while

$$\rho = \alpha \qquad \text{on } Y = 0, \tag{2.20g}$$

$$\theta_Y = 0 \qquad \text{on } Y = 1. \tag{2.20h}$$

The porosity, $\phi(R) = 1-\pi(r_0+R)^2$, surface area, $C(R) = 2\pi(r_0+R)$, and effective diffusivity, $\mathcal{D}(R)$ (given by (A 4)), all vary with the thickness of the deposited dirt layer.

We assume that, initially, the porous material is entirely saturated with a uniform liquid–dirt mixture, none of which has yet deposited (ie: the timescale of deposition is assumed longer than the timescale over which the liquid–dirt mixture flooded the material). Thus at $T = 0$,

$$R = 0, \quad H = 0, \quad \theta = \theta_{IC}. \tag{2.21}$$

Our homogenised model (2.20) is similar in structure to those proposed in Breward *et al.* (2020), Sanaei *et al.* (2022), and Ji & Sanaei (2023), with the suspended dirt satisfying a reaction–diffusion equation ahead of a moving evaporation front. However, through the systematic homogenisation analysis, we have found the correct form for the diffusion term in (2.20*b*), which was erroneously given as $(D(\phi\theta)_Y)_Y$ (in our notation) by Ji & Sanaei (2023). Additionally, we have quantified the effective parameters $\mathcal{D}$, C, and ϕ, which all vary with the deposited dirt layer thickness R. We also impose different boundary conditions to Ji & Sanaei (2023), which will result in different drying behaviours, as discussed in section 3 below.

A key assumption of our homogenisation analysis was that $\sigma = O(1)$, which ensured that θ (and therefore R) is uniform to leading order on the microscale. As discussed further in section A.2 of the appendix, the extremely slow suspended dirt diffusion limit of $\sigma = O(\epsilon^{-1})$ is not captured by this model: in this case we would expect non-periodic behaviour on the microscale at the evaporating interface, and the homogenisation analysis would break down. We do not consider this situation here.

3. An ODE for the motion of the evaporation front

The parameter $\delta = \rho^*/\rho_L$ is generally small; indeed for water evaporating we expect $\delta \approx 10^{-3}$. Before studying the full drying problem, we consider the limit of $\delta \to 0$ in the vapour-gas transport problem, which we will show results in a single ODE describing the motion of the evaporation front $H(T)$. This gives insight into the drying dynamics and is interesting as a comparison with other models for the motion of evaporating interfaces in the literature, eg Ji & Sanaei (2023). Furthermore, the analysis in this section is helpful for all of the subsequent analysis of the model, including the early-time asymptotic analysis in the following section (section 4), which we will use to initialise numerical simulations of the model.

For small δ we see from (2.20*a*) that the vapour density profile is quasi-steady, varying instantaneously with the motion of the evaporation front. Specifically, in the limit $\delta \to 0$, the

vapour transport equation (2.20*a*) becomes

$$-\nu\phi|_H H_T \rho_Y = (\mathcal{D}\rho_Y)_Y. \tag{3.1}$$

Integrating twice with respect to Y, and applying the boundary conditions (2.20*d*) and (2.20*g*) we obtain

$$\rho = \frac{1}{\nu}\left(1 - (1-\nu\alpha)\exp\left(-\nu\phi|_H H_T \int_0^Y \frac{1}{\mathcal{D}(R(\hat{Y}))}\,\mathrm{d}\hat{Y}\right)\right). \tag{3.2}$$

By additionally imposing the boundary condition (2.20*e*) we obtain an equation for the motion of the evaporation front, H, in terms of the suspended dirt volume fraction there, $\theta|_H$, namely

$$H_T \int_0^H \frac{1}{\mathcal{D}(R(\hat{Y}))}\,\mathrm{d}\hat{Y} = \frac{1}{\nu\phi|_H}\log\left(\frac{1-\nu\alpha}{1-\nu f(\theta|_H)}\right). \tag{3.3}$$

One particular case of interest is if $\mathcal{D}$ is uniform (for instance if little dirt has been deposited, so $R \approx 0$ is constant). In this case (3.3) reduces to

$$HH_T = \frac{\mathcal{D}}{\nu\phi|_H}\log\left(\frac{1-\nu\alpha}{1-\nu f(\theta|_H)}\right). \tag{3.4}$$

If $\theta|_H$ were constant, we would see a $\sqrt{T}$ behaviour of the evaporation front, as expected for this type of Stefan problem. For $\mathcal{D}$ non-uniform in Y, the integral term in (3.3) behaves like an overall resistance to vapour transport. In particular, the integral is dominated by any localised regions of porespace in $Y < H$ for which $\mathcal{D}$ is very small.

We see that the ODE (3.4) for H (with $\mathcal{D}$ constant) takes the form

$$HH_T = E_1(\phi|_H, \theta|_H), \tag{3.5}$$

for an algebraic function E_1, while the more general (3.3) takes the form

$$H_T = E_2(\phi|_H, \theta|_H, H, R|_{Y<H}). \tag{3.6}$$

By comparison, Ji & Sanaei (2023) prescribe an evaporative flux that does not explicitly depend on H, of the form

$$H_T = E_3(\phi|_H, \theta|_H), \tag{3.7}$$

in our notation. Unlike (3.5) and (3.6), the model (3.7) does not explicitly depend on the position H of the evaporating interface. These different equations for H result from different modelling assumptions: Ji & Sanaei (2023) assume that the vaporisation of the liquid molecules is the limiting process in the evaporation, whereas we have assumed that the vaporisation is instantaneous (the vapour is at its saturation point adjacent to $Y = H$) and that evaporation is instead limited by the transport of vapour out of the porous material. For sufficiently deep or hydrophobic porous media that there is a moving drying front, it is clear that the evaporation rate should depend on the location H of the drying front (Lehmann *et al.* 2008; Shokri *et al.* 2008). Furthermore, we note that our drying model is given in terms of well-defined physical parameters such as the diffusivity and saturation vapour densities, and results in a reasonable drying timescale $l^2\rho_L/\rho_* D_v \approx 10^2$ seconds (using values for water: $\rho_L \approx 10^3\,\mathrm{kg\,m^{-3}}$, $\rho_* \approx 1\,\mathrm{kg\,m^{-3}}$, $D_v \approx 10^{-5}\,\mathrm{m^2\,s^{-1}}$, and $l \sim 10^{-3}\,\mathrm{m}$), whereas the coefficients in a prescribed evaporation rate must be fitted in some way.

We note from (3.3) that evaporation only occurs when $f(\theta|_H) > \alpha$, so that the vapour density at the liquid–gas interface is greater than the atmospheric vapour density; otherwise if $f(\theta|_H) = \alpha$ we see that $H_T = 0$. We define $\hat{\theta}$ such that $f(\hat{\theta}) = \alpha$, noting that since f is monotonic in θ, evaporation only occurs for $\theta < \hat{\theta}$.

Our analysis above (and in the remainder of this paper) is for the case that the atmospheric

vapour density $\rho = \alpha$ is prescribed at the surface $Y = 0$. As an aside, we now briefly consider an alternative case, in which the flux, J, of vapour out of the material at $Y = 0$ is prescribed by a Newton cooling law: $J = m(\rho|_0 - a_\infty)$, for some constants a_∞ (the far-field ambient vapour density) and m (the mass-transfer coefficient). Since the vapour flux is spatially uniform throughout $Y < H$ in the limit $\delta \ll 1$, we find that $\phi|_H H_T = m(\rho|_0 - a_\infty)$. Eliminating $\rho|_0$, we find that H_T is given by the implicit ODE

$$H_T \int_{Y=0}^{H} \frac{1}{\mathcal{D}}\,\mathrm{d}Y = \frac{1}{\nu\phi|_H} \log\left(\frac{1 - \nu a_\infty - \nu\phi|_H H_T/m}{1 - \nu f(\theta|_H)}\right). \tag{3.8}$$

(We may rearrange (3.8) to give H_T explicitly in terms of a Lambert-W function, but we consider the form (3.8) more useful as we may compare directly with (3.3).) Clearly in the limit as $m \to \infty$ (for which vapour is easily removed from the surface of the porous material), and with $a_\infty = \alpha$ we regain (3.3). For bounded mass-transfer coefficient m, the non-instantaneous removal of vapour from the surface results in a slower evaporation rate H_T, compared with that given by (3.3).

4. Early-time behaviour and numerical method

In this section we first consider the early-time behaviour of our model (2.20) in section 4.1, in the limit of $\delta \ll 1$. This will be necessary in order to accurately initialise numerical simulations of the model, which is then discussed in section 4.2.

4.1. *Early-time analysis*

To study the early-time behaviour of the system (2.20), we suppose $T = b\tau$ where $b \ll 1$ is the smallest parameter in the system, and $\tau = O(1)$. From (2.20*c*), on this timescale we see that $R_\tau = O(b\kappa) \ll 1$, and so R is small, hence all of $\mathcal{D}, \phi$, and C are constant to leading order in b.

We first consider the vapour problem in $Y < H$. On the short timescale the interface only moves a short distance, and so we rescale

$$H = \sqrt{\frac{b\mathcal{D}}{\phi}}\bar{H} \qquad Y = \sqrt{\frac{b\mathcal{D}}{\phi}}\bar{Y}, \tag{4.1}$$

in order to balance the mass-flux boundary condition (2.20*d*). The vapour problem is therefore self-similar in that we regain the same system at early time with these rescalings as the full system (2.20*a*), (2.20*d*)-(2.20*e*) and (2.20*g*), namely

$$\delta\rho_\tau - (\nu - \delta)\bar{H}_\tau\rho_{\bar{Y}} = \rho_{\bar{Y}\bar{Y}}, \qquad \text{for } \bar{Y} \in (0, \bar{H}(\tau)), \tag{4.2a}$$

$$\rho = \alpha \qquad \text{on } \bar{Y} = 0, \tag{4.2b}$$

$$\rho_{\bar{Y}} = (1 - \nu\rho)\bar{H}_\tau \qquad \text{on } \bar{Y} = \bar{H}(\tau), \tag{4.2c}$$

$$\rho = f(\theta) \qquad \text{on } \bar{Y} = \bar{H}(\tau). \tag{4.2d}$$

We have already noted that $\delta \ll 1$ in general, and we take this limit now to make analytical progress. As in section 3 we find

$$\rho = \frac{1}{\nu}\left(1 - (1 - \nu\alpha)\exp\left(-\nu\bar{H}_\tau\bar{Y}\right)\right), \tag{4.3}$$

where $\bar{H}(\tau)$ is the solution of

$$\bar{H}\bar{H}_\tau = \frac{1}{\nu}\log\left(\frac{1 - \nu\alpha}{1 - \nu f(\theta|_{\bar{Y}=\bar{H}(\tau)})}\right). \tag{4.4}$$

The value of θ at $\bar{Y} = \bar{H}(\tau)$ depends on the solution of the suspended dirt problem in the domain $Y \in (H, 1) = (\sqrt{b\mathcal{D}/\phi}\,\bar{H}(\tau), 1)$. On this short timescale, the full dirt problem (2.20*b*), (2.20*f*) and (2.20*h*), with the initial condition (2.21), becomes

$$\sigma\phi\theta_\tau = b\big(\mathcal{D}\theta_{YY} - \sigma\kappa C(\theta_* - \theta)(\theta - \beta\chi_R)\big) \qquad \text{for } Y \in (\sqrt{b\mathcal{D}/\phi}\,\bar{H}(\tau), 1), \tag{4.5a}$$

$$\sigma\phi\theta\bar{H}_\tau + \sqrt{b}\mathcal{D}\theta_Y = 0 \qquad \text{on } Y = \sqrt{b\mathcal{D}/\phi}\,\bar{H}(\tau), \tag{4.5b}$$

$$\theta_Y = 0 \qquad \text{on } Y = 1, \tag{4.5c}$$

$$\theta = \theta_{IC} \qquad \text{at } \tau = 0. \tag{4.5d}$$

To leading order in b we see that $\theta_\tau = 0$, so that $\theta = \theta_{IC}$ is independent of time over the domain. However, in a boundary layer at $Y = \sqrt{b\mathcal{D}/\phi}\bar{H}$, suspended dirt accumulates due to the motion of the evaporation front. To examine this region, we make the change of variables $Y = \sqrt{b\mathcal{D}/\phi}(\bar{H}(\tau) + z)$, so that, at leading order in b, the equations are

$$\sigma\left(\theta_\tau - \bar{H}_\tau\theta_z\right) = \theta_{zz} \qquad \text{for } z > 0, \tag{4.6a}$$

$$\sigma\theta\bar{H}_\tau + \theta_z = 0 \qquad \text{on } z = 0, \tag{4.6b}$$

$$\theta \to \theta_{IC} \qquad \text{as } z \to \infty, \tag{4.6c}$$

$$\theta = \theta_{IC} \qquad \text{at } \tau = 0. \tag{4.6d}$$

This system (4.6) must be solved with (4.4) to determine θ and $\bar{H}$.

We look for a similarity solution of the form

$$\bar{H} = \frac{2\lambda}{\sqrt{\sigma}}\sqrt{\tau}, \qquad \theta = \Theta\left(\frac{\sqrt{\sigma}z}{\sqrt{\tau}}\right), \tag{4.7}$$

for some constant λ to be determined. In particular, from (4.4) we see that the suspended dirt volume fraction at the evaporating interface, $\theta|_{\bar{H}} = \Theta(0)$, must be constant in time for such a similarity solution to exist. Substituting into (4.6), we find the solution

$$\Theta = \theta_{IC} + (\Theta(0) - \theta_{IC})\,\frac{\operatorname{erfc}\left(\lambda + \frac{\sqrt{\sigma}z}{2\sqrt{\tau}}\right)}{\operatorname{erfc}(\lambda)}, \tag{4.8}$$

where λ and the constant $\Theta(0)$ satisfy

$$\lambda^2 = \frac{\sigma}{2\nu}\log\left(\frac{1 - \nu\alpha}{1 - \nu f(\Theta(0))}\right), \tag{4.9}$$

$$\Theta(0) = \theta_{IC} + \sqrt{\pi}\lambda\Theta(0)e^{\lambda^2}\operatorname{erfc}(\lambda). \tag{4.10}$$

Solutions of (4.9)–(4.10) may be computed numerically, and are shown for various σ and θ_{IC} in figure 2.

To establish some intuitive understanding of this early-time behaviour, we now consider the sublimits $\sigma \ll 1$, $\theta_{IC} \ll 1$, and $\sigma \gg 1$ in turn. We show our early-time analytic solutions for each case in figure 3 (alongside numerical solutions for comparison, computed using the method described in section 4.2 below), all with excellent agreement. In each, we see that the vapour density ρ varies from $f(\theta|_H) = 1 - \theta|_H$ at $Y = H$ to $\alpha = 0$ at the surface of the material, according to (4.3). The evaporation front moves with the expected $\sqrt{T}$ behaviour, faster if there is a steeper vapour-density gradient. Suspended dirt accumulates in the liquid ahead of the evaporation front, with a spatial maximum in θ at $Y = H$. The size of the boundary layer at H over which θ varies is dependent on σ, which quantifies suspended dirt diffusion. At early times, we expect little dirt deposition, so that the dirt-layer thickness $R \approx 0$ throughout the porous material.

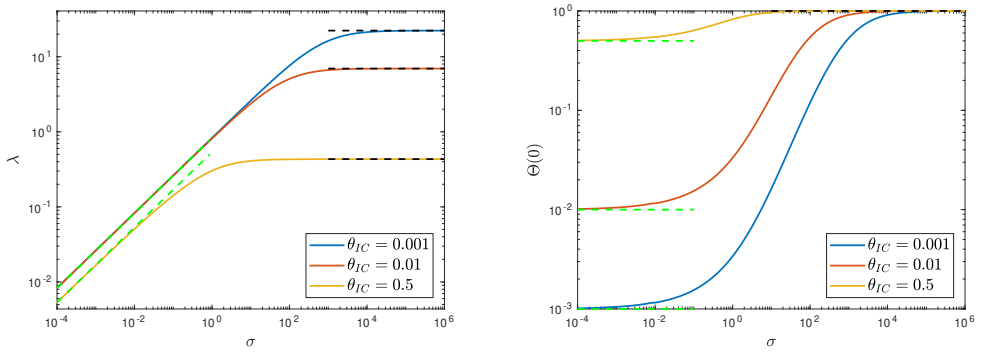

Figure 2: Early-time solution behaviour. Coloured lines show the variation of the solution of (4.9) and (4.10) with the suspended dirt diffusion timescale σ. Green dashed lines are the small-σ approximations (4.11), while black dashed lines are the large-σ approximations (4.13). Here we use the form $f(\theta) = 1 - \theta$ and set $\alpha = 0$, so that $\hat{\theta} = 1$. We additionally set $\nu = 0.5$.

If $\sigma \ll 1$ so that suspended dirt diffusion is fast relative to the motion of the evaporation front, then we see from (4.9) that $\lambda = O(\sqrt{\sigma})$, and so from (4.10) that $\theta|_h \sim \theta_{IC}$. Specifically, we find that

$$\left.\begin{aligned} \Theta(0) &= \theta_{IC} + O(\sqrt{\sigma}), \\ \lambda &= \sqrt{\sigma}\left(\sqrt{\frac{1}{2\nu}\log\left(\frac{1-\nu\alpha}{1-\nu f(\theta_{IC})}\right)} + O(\sqrt{\sigma})\right) \end{aligned}\right\} \qquad \text{as } \sigma \to 0. \tag{4.11}$$

Thus, reverting to our original variables, the early-time evaporating interface is given by

$$H = \sqrt{T}\sqrt{\frac{\mathcal{D}}{2\nu\phi}\log\left(\frac{1-\nu\alpha}{1-\nu f(\theta_{IC})}\right)} + O(\sqrt{\sigma}) \qquad \text{as } \sigma \to 0. \tag{4.12}$$

We also note from the form (4.8) of the solution that the spatial region over which θ varies is wide, $O(1/\sqrt{\sigma})$. In this small-σ limit, the diffusion of dirt is fast relative to the motion of the evaporation front, and so the suspended dirt volume fraction θ remains close to its initial value θ_{IC}, only deviating by a small, $O(\sqrt{\sigma})$, amount. For conservation of overall dirt, the region over which the accumulating suspended dirt is spread is wide, of $O(1/\sqrt{\sigma})$ relative to the early-time boundary layer. This may be seen in figure 3a–b: since $\sigma \ll 1$ the θ-profile is approximately uniform in Y, and so close to its initial value of $\theta_{IC} = 0.1$ at early times. The suspended dirt is accumulating due to the evaporation, but spread almost evenly through the domain.

Next, we suppose that $\sigma = O(1)$ but the initial suspended dirt volume fraction $\theta_{IC} \ll 1$ is small. In this case, for a balance in both of (4.9) and (4.10) we must have $\Theta(0) = O(\theta_{IC})$, and $\lambda = O(1)$, as we might expect. The solution shown in figure 3c–d is for this case, with $\theta_{IC} = 0.1$: we indeed observe that $\theta|_H = O(0.1)$ (and this effect becomes increasingly clear for smaller θ_{IC}).

Finally, if $\sigma \gg 1$, so that the diffusion of suspended dirt is slow relative to the motion of the evaporation front, then from (4.9) we see that we must have $f(\Theta(0)) = \alpha$ to leading order in $\sigma^{-1} \ll 1$. At this value,

$$\Theta(0) = \hat{\theta}, \tag{4.13a}$$

there is no evaporation at leading order, as the vapour density at the atmospheric value is

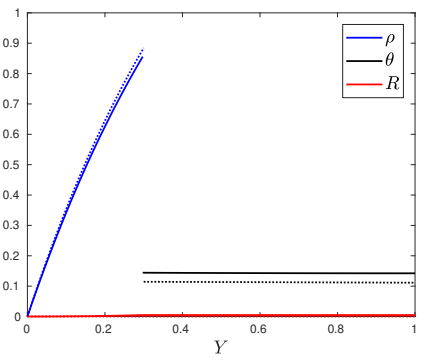

(a)

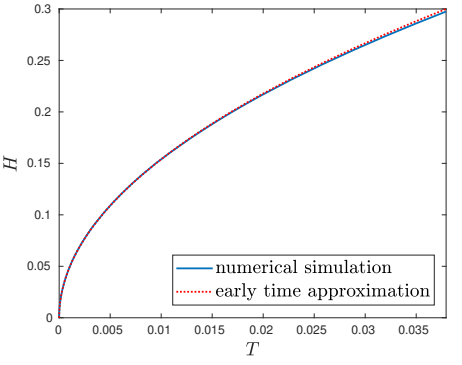

(b)

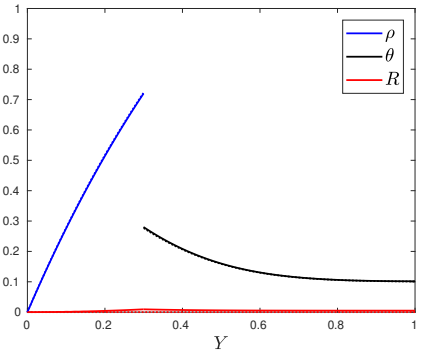

(c)

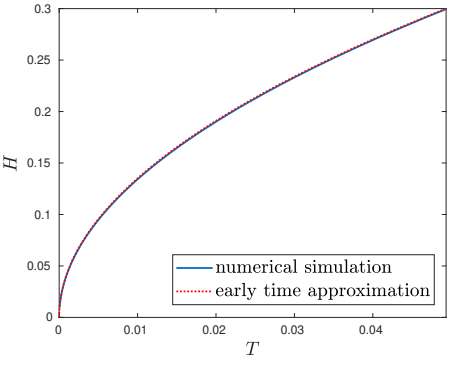

(d)

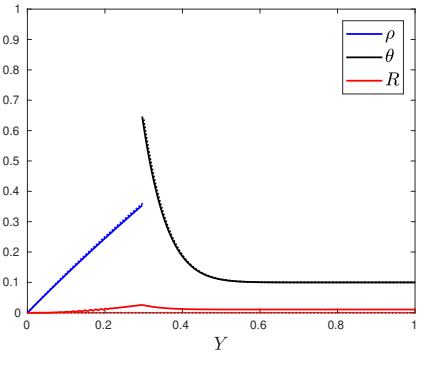

(e)

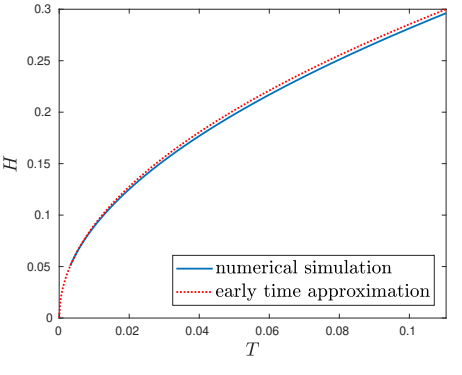

(f)

Figure 3: Early-time solutions (4.3),(4.7), and (4.8) (dotted lines) compared with numerical solutions (solid lines) of the full model (2.20), for $\sigma = 0.01$ (top) $\sigma = 1$ (middle) and $\sigma = 10$ (bottom). The profiles of ρ, θ and R in figures a, c, and e are at times for which $H = 0.3$ (towards the end of what we would consider "early" time, especially in the small-σ case). Throughout the figure we take $f(\theta) = 1 - \theta$, $\kappa = 1$, $\theta_{IC} = 0.1$, $\nu = 0.5$, $\delta = 10^{-3}$, $r_0 = 0.2$, $\alpha = 0$, and $\beta = 0$.

in equilibrium with the liquid–dirt interface, and there is no transport of vapour out of the porous material. Indeed, we see from (4.10) that when $\theta = \hat{\theta}$, λ is the solution of

$$\lambda e^{\lambda^2} \mathrm{erfc}(\lambda) = \frac{\hat{\theta} - \theta_{IC}}{\hat{\theta}\sqrt{\pi}}, \tag{4.13b}$$

which is independent of σ and of $O(1)$, so that the position of the evaporating interface, given by

$$H = \frac{2\lambda}{\sqrt{\sigma}} \sqrt{\frac{\mathcal{D}}{\phi}} \sqrt{T}, \tag{4.14}$$

is of order $\sigma^{-1/2} \ll 1$ away from its initial position. Thus when the suspended dirt diffusion is slow, the diffusion of dirt away from H limits the speed of the evaporation front, so that there is a slower, $O(\sigma)$, drying timescale. We also note from (4.8) that the region over which θ varies is narrow, with width $O(1/\sqrt{\sigma})$ relative to the early-time boundary layer. The boundary-layer is narrow for large σ, so that the early-time solution actually remains valid for the majority of the drying process. Indeed, in figure 3e–f we see excellent agreement between the early-time analytic solution and the numerical solution for ρ, θ and H up to the time when the evaporating front is halfway through the domain. This is because the boundary layer at H over which θ varies is narrow, and so the effect of the boundary at $Y = 1$ is not felt until H is close to 1. However, we notice in figure 3e that the early-time approximation $R = 0$ ceases to be accurate at these late times. The early-time solution would remain valid so long as R remains relatively small (eg: if κ and θ_{IC} are fairly small). We note that, since the boundary layer width scales with $\sqrt{T}$, it quickly becomes numerically impractical to resolve the solution at small times for large σ. The early-time asymptotic solution is therefore very valuable in initialising the simulations accurately for large σ.

Finally, we note that our early-time analysis in this section is equivalent to studying the original problem on a semi-infinite domain $Y \in (0, \infty)$, in the combined limit $\kappa, \delta \to 0$.

4.2. *Numerical method*

We solve the model (2.20) numerically using the method of lines. Specifically, we first transform the model onto two separate fixed domains, setting $\eta = Y/H(T)$ for the gas–vapour problem, which then holds in $\eta \in (0, 1)$, and setting $\xi = (Y - H(T))/(1 - H(T))$ for the liquid–dirt problem, which then also holds in $\xi \in (0, 1)$. We discretise spatially on these transformed domains, with a uniform mesh, using central differences for diffusive terms and first-order upwinding for advective terms, so that the scheme is overall first order. (The advection for the vapour problem (2.20*a*), including the artificial advection terms due to the change of variables, is negative; the purely artificial advection in the liquid–dirt problem (2.20*b*)–(2.20*c*) is also negative. Upwinding these terms therefore requires forward differences in both cases.) We then use the inbuilt ODE solver ode15s in Matlab for the timestepping. We note that the model is stiff in certain parameter regimes of interest ($\delta \ll 1$ and/or $\sigma \ll 1$), and that ode15s is specifically designed for stiff-systems. Ode15s is a multistep solver, using numerical differentiation formulas of order 1–5 (Shampine & Reichelt 1997). We make use of our early-time asymptotic solution of section 4.1 to initialise our numerical simulations. In particular the spatial mesh must be sufficiently fine to resolve the boundary layer in the suspended dirt problem at $Y = H$ at early times. Our analysis in section 4.1 suggests we require the number of spatial meshpoints N to scale like

$$N = O\left(\sqrt{\frac{\mathcal{D}(0)\sigma}{\phi(0)T}}\right) \quad \text{for } T \ll 1. \tag{4.15}$$

More efficient solvers might take further advantage of the asymptotic structure of the system and distribute meshpoints unevenly through the domain in order to ensure good resolution of the boundary layer while maintaining computational efficiency. However, by making use of our early-time asymptotic solution we do not require simulations at particularly small T, and our uniform-mesh formulation suffices.

5. The slow-deposition limit $\kappa \ll 1$ and dry-clogging

Having stated the model and our numerical solution method, we are now in a position to explore solutions of the model. In this section, we focus on the limit $\kappa \ll 1$, for which the dirt deposition timescale is much longer than the evaporation timescale. We expect that the accumulation of suspended dirt due to evaporation and the effects of suspended dirt diffusion to be dominant.

We first consider the leading-order behaviour, taking $\kappa = 0$, and show that the evaporation becomes infinitely slow as suspended dirt accumulates. We then allow κ to be small but non-zero, and explore our first clogging scenario, which we term "dry-clogging".

5.1. *Infinitely slow evaporation when* $\kappa = 0$

Taking $\kappa = 0$, we see from (2.20*c*) that we have $R = 0$ everywhere, and thus $\mathcal{D} = \mathcal{D}_0$, $C = C_0$, and $\phi = \phi_0$ are all constant, equal to their values at $R = 0$. Taking the $\delta \ll 1$ limit as in section 3, the motion of the evaporation front is therefore governed by (3.4), ie:

$$HH_T = -\frac{\mathcal{D}_0}{\nu\phi_0}\log\left(\frac{1-\nu f(\theta|_H)}{1-\nu\alpha}\right), \tag{5.1}$$

while θ satisfies

$$\frac{\sigma\phi_0}{\mathcal{D}_0}\theta_T = \theta_{YY} \qquad \text{for } Y \in (H(T), 1), \tag{5.2a}$$

$$\frac{\sigma\phi_0}{\mathcal{D}_0}\theta H_T + \theta_Y = 0 \qquad \text{on } Y = H(T), \tag{5.2b}$$

$$\theta_Y = 0 \qquad \text{on } Y = 1, \tag{5.2c}$$

$$\theta = \theta_{IC} \qquad \text{at } T = 0. \tag{5.2d}$$

To investigate how the accumulation of suspended dirt affects the evaporation rate, we consider the additional limit of $\sigma \ll 1$ so that the diffusion of suspended dirt is fast. In this case, we see from (5.2) that $\theta(T)$ is uniform, and so, for overall conservation of dirt, we must have

$$\theta(T) = \frac{\theta_{IC}}{1-H(T)}. \tag{5.3}$$

Substituting (5.3) into (5.1) we obtain the single equation for $H(T)$

$$HH_T = -\frac{\mathcal{D}_0}{\nu\phi_0}\left[\log\left(1-\nu f\left(\frac{\theta_{IC}}{1-H}\right)\right) - \log(1-\nu\alpha)\right]. \tag{5.4}$$

As discussed previously, the evaporation shuts down when $\theta = \hat{\theta}$ so that $f(\hat{\theta}) = \alpha$, since then $H_T = 0$. At this point we see from (5.3) that $H = 1 - \theta_{IC}/\hat{\theta}$.

Numerical solutions of the model (2.20) (with $\kappa = 0$, $\delta = 10^{-3}$) are shown in figures 4a and b, and compared with the solution of (5.4) for the limit of $\sigma \to 0$, with good agreement for $\sigma = 0.1$ and smaller. We take the functional form $f(\theta) = 1 - \theta$ for these simulations, and fix $\alpha = 0$ (so that $\hat{\theta} = 1$). In figure 4c, we show solutions of (5.4) for various θ_{IC}. We see

that, for larger θ_{IC}, the evaporation is slower, with the evaporating interface H moving more slowly into the domain. In particular we note that when $\theta_{IC} = 0$ the evaporation is completed (with $H = 1$) in finite time

$$T = -\frac{\nu\phi_0}{2\mathcal{D}_0 \log(1-\nu)} \approx 0.36, \tag{5.5}$$

(from (5.4) with $\theta_{IC} = 0$), whereas for $\theta_{IC} > 0$ we see that H appears to take infinite time to reach $1 - \theta_{IC}/\hat{\theta}$.

We investigate this late-time behaviour (within the $\sigma \ll 1$ limit) by considering the expansion

$$H = 1 - \frac{\theta_{IC}}{\hat{\theta}}(1 + c\mathcal{H}) \qquad \text{so that} \qquad \theta = \frac{\hat{\theta}}{1 + c\mathcal{H}}, \tag{5.6}$$

where $c \ll 1$ is small and $\mathcal{H} = O(1)$ is positive. Assuming that f is continuous at $\theta = \hat{\theta}$, on substitution of (5.6) into (5.4) we find (retaining only leading-order terms on either side)

$$\begin{aligned} c\left(1 - \frac{\theta_{IC}}{\hat{\theta}}\right)\frac{\theta_{IC}}{\hat{\theta}}\mathcal{H}_T &= -\frac{\mathcal{D}_0}{\phi_0(1-\nu\alpha)}\left(f\left(\frac{\hat{\theta}}{1+c\mathcal{H}}\right) - \alpha\right) \\ &= -\frac{\mathcal{D}_0}{\phi_0(1-\nu\alpha)}\left(f\left(\hat{\theta}(1 - c\mathcal{H} + O(c^2))\right) - \alpha\right). \end{aligned} \tag{5.7}$$

So long as the gradient of the function f is bounded at $\hat{\theta}$, we may Taylor expand the right hand side of (5.7) and thus find that, to leading order in c,

$$\mathcal{H}_T = \frac{\mathcal{D}_0\hat{\theta}^3}{\phi_0(1-\nu\alpha)\theta_{IC}(\hat{\theta} - \theta_{IC})} f'(\hat{\theta})\mathcal{H}, \tag{5.8}$$

since $f(\hat{\theta}) = \alpha$ by definition. Thus $\mathcal{H}$ decays exponentially to zero as $T \to \infty$ (since $f'(\hat{\theta}) < 0$) and the evaporation takes infinite time. (Similarly if $f'(\hat{\theta}) = 0$ but higher derivatives are non-zero then $\mathcal{H}$ has polynomial, and still infinite-time, decay.)

We might ask if there are sensible choices for $f(\theta)$ that result in finite-time completion of the evaporation. In order for the evaporation to complete in finite time, we see that the gradient of f must be unbounded at $\hat{\theta}$. For instance if $f(\hat{\theta}(1 - c\mathcal{H})) = \alpha + A(c\mathcal{H})^{1/n}$, for $n > 1$ and some constant A, then by substituting this expansion for f into (5.7) and integrating the resulting ODE for $\mathcal{H}$ in time T, we find that

$$\mathcal{H} \sim \left(\text{constant} - \frac{D_0\hat{\theta}^2 A(n-1)}{\phi_0\theta_{IC}(\hat{\theta} - \theta_{IC})(1-\nu\alpha)n} c^{-(n-1)/n} T\right)^{n/(n-1)}, \tag{5.9}$$

and so $\mathcal{H}$ reaches zero in finite time. However, this finite-time drying requires that the gradient of f is unbounded at $\hat{\theta}$, which is physically unreasonable, not least because $\hat{\theta}$ (defined as the value of θ for which $f = \alpha$) depends on the atmospheric vapour density ρ_a via the value of α. For physically reasonable functional forms $f(\theta)$, we therefore expect a bounded derivative at $\hat{\theta}$, and thus that the evaporation becomes unboundedly slow as $\theta \to \hat{\theta}$.

This analysis is for the case $\sigma \ll 1$. For larger σ, we see from figure 4a that the evaporation rate is slower. As we see in figure 4b, this is because suspended dirt accumulates near the evaporating interface rather than quickly diffusing through the domain, and with higher values of $\theta|_H$, we see from (5.1) that the evaporation rate is reduced. Numerically, we see that, for non-negligible σ, we still have $H \to 1 - \theta_{IC}/\hat{\theta}$ in infinite time. Indeed, although for larger σ the evaporation is additionally slowed by the diffusion of the suspended dirt away from the evaporating interface, at late times when the evaporation becomes infinitely slow, the diffusion of dirt does not limit the drying process.

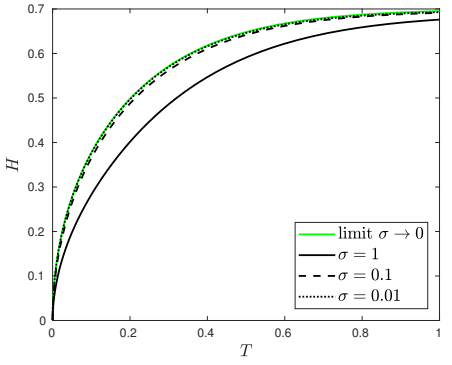

(a) Motion of the evaporation front $H(T)$ for various σ, with $\theta_{IC} = 0.3$.

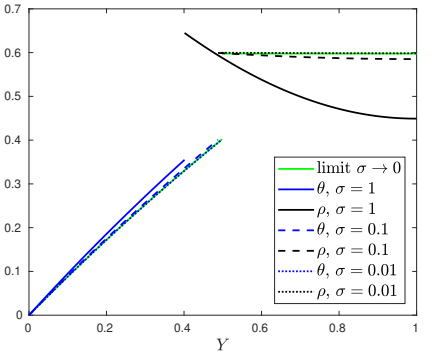

(b) Vapour density and suspended dirt volume fraction profiles at the same time $T = 0.2$ for various σ, with $\theta_{IC} = 0.3$.

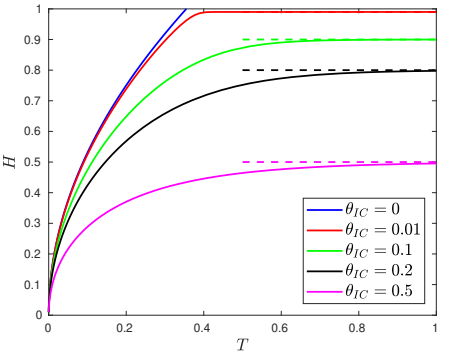

(c) Effect of θ_{IC} on the evaporating interface motion. Dashed lines are $1 - \theta_{IC}$.

Figure 4: The effect of suspended dirt accumulation on the evaporation, for $\kappa = 0$ and $\sigma \ll 1$. Numerical solutions of (2.20) shown with $\kappa = 0$ (no dirt deposition), alongside the solution of (5.4) in the limit $\sigma \to 0$, (taking $f(\theta) = 1 - \theta$ and $\alpha = 0$). Throughout the figure we take $\nu = 0.5$ and $r_0 = 0.2$.

In summary, for $\kappa = 0$ the drying takes infinite time to complete and, as drying occurs, the suspended dirt concentrates in a layer at $y = 1$. The drying never fully stops (although it becomes infinitely slow). By contrast we will see in section 5.2 that if $\kappa \ll 1$ is non-zero then the dirt begins to deposit at late time, and this causes the drying to completely stop in finite time (which we refer to as clogging).

5.2. *Dry-clogging behaviour for small but non-zero* κ

The analysis in section 5.1 assumed that $\kappa = 0$ so that there was no deposition of dirt at all, and we saw that, in this case, there is an infinitely long drying time as $\theta \to \hat{\theta}$. However, in reality we might instead have $\kappa \ll 1$ small but non-zero. In this case, we would expect the same behaviour as in section 5 initially (over an $O(1)$ time), but then during the slow evolution towards $\theta \to \hat{\theta}$, the deposition will begin to become important. Dirt is slowly deposited, and the deposited dirt layer, thickness R, grows. From the microscale geometry, we see that, when $R = R_{\text{clog}} := 0.5 - r_0$, the dirt layers on neighbouring solid circles meet, and

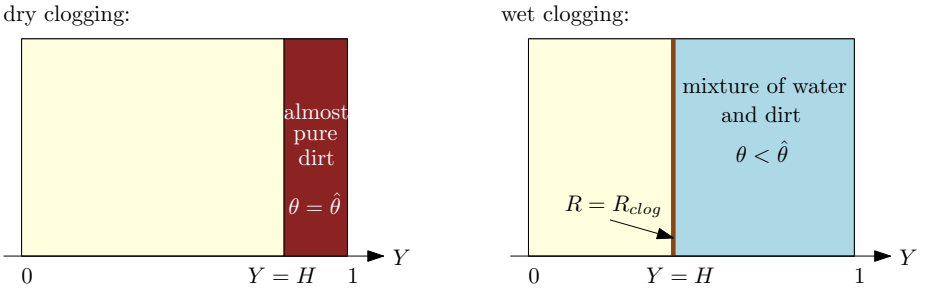

Figure 5: The two clogging behaviours: dry clogging (left) for which $\theta = \hat{\theta}$ for $Y > H$ when the system clogs, so that (almost) pure dirt remains with negligible liquid trapped; and wet clogging (right) for which a mixture of liquid and dirt is trapped in $Y > H$ by the clogging.

the pore-scale liquid region ceases to be connected. This means that the effective diffusivity $\mathcal{D}(R_{\rm clog}) = 0$. In particular, if $R = R_{\rm clog}$ then vapour cannot be transported through the porous material, and thus evaporation ceases. We define "clogging" to be this situation when $R = R_{\rm clog}$ at $Y = H(T)$ at finite time T, and thus the evaporation is stopped.

To investigate this, we look at the behaviour of the system on the long time $T = \tilde{T}/\kappa$ over which R varies. With this change of variables in (5.1), we see that H satisfies

$$\kappa H_{\tilde{T}} \int_0^H \frac{1}{\mathcal{D}}\,\mathrm{d}Y = -\frac{1}{\nu\phi}\log\left(\frac{1-\nu f(\theta|_H)}{1-\nu\alpha}\right), \tag{5.10}$$

while for $Y > H$

$$R_{\tilde{T}} = \theta - \beta\chi_R, \tag{5.11}$$

$$\kappa\sigma\phi\theta_{\tilde{T}} = (\mathcal{D}\theta_Y)_Y - \sigma\kappa\mathcal{C}(\theta_* - \theta)(\theta - \beta\chi_R), \tag{5.12}$$

along with the boundary conditions (2.20*f*) and (2.20*h*)

$$\kappa\sigma\phi H_{\tilde{T}}\theta + \mathcal{D}\theta_Y = 0 \qquad \text{on } Y = H(\tilde{T}), \tag{5.13}$$

$$\theta_Y = 0 \qquad \text{on } Y = 1. \tag{5.14}$$

At leading order in κ, we see from (5.12)–(5.14) that $\theta = \hat{\theta}$ is uniform, and thus, in $Y > H$, from (5.11) we find that

$$R = (\hat{\theta} - \beta)\tilde{T}, \tag{5.15}$$

is spatially uniform. Clearly $R = R_{\rm clog}$ after time $\tilde{T} = R_{\rm clog}/(\hat{\theta} - \beta)$, or in the original time variable, at

$$T_{\rm end} = \frac{R_{\rm clog}}{\kappa(\hat{\theta} - \beta)} + O(1). \tag{5.16}$$

We note that, during this late, $O(1/\kappa)$ time, the position of the evaporating interface, H, and the $O(\kappa)$ deviation of θ from $\hat{\theta}$ may be found by going to next order in κ in (5.10) and (5.12), and matching to the early-time behaviour in $\tilde{T}$ (or $O(1)$ time behaviour in T). Thus R reaches the clogging point $R_{\rm clog}$ in finite time, and thus the system clogs. We term this type of clogging "dry"-clogging because, to leading order, $\theta = \hat{\theta}$ everywhere ahead of the clogging front. Since we expect $\hat{\theta} \approx 1$ (indeed we take $\hat{\theta} = 1$ in our numerical simulations), there is therefore a negligible amount of liquid left trapped in the porous material by the clogging. This dry-clogging behaviour is illustrated in figure 5 (left).

Results of a numerical simulation of (2.20) for $\kappa = 0.04$ are shown in figure 6. As expected, we see in figure 6b that H varies from zero to around $1 - \theta_{IC}/\hat{\theta}$ over an $O(1)$ time, while R

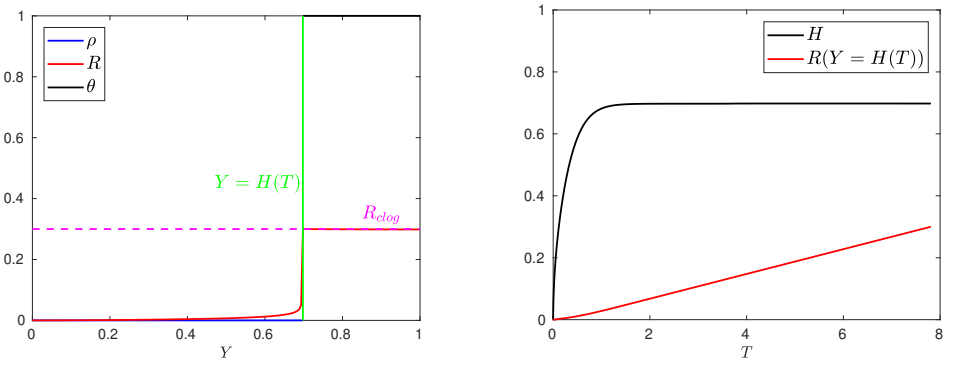

(a) (b)

Figure 6: Numerical solution of (2.20) for small κ showing dry-clogging behaviour, using parameter values $\kappa = 0.04$, $\sigma = 1$, $\theta_{IC} = 0.3$. (a): Profiles of ρ, θ, and R very close to the clogging time T_{end}. (b): The motion $H(T)$ of the evaporation front.

at the interface $Y = H$ (where R is maximised in space at that time T) remains closer to zero during the time for which H varies. Subsequently, there is a longer $O(1/\kappa)$ time over which H remains nearly stationary, since $\theta \approx \hat{\theta}$ everywhere in $Y > H$, while R (at $Y = H$) increases linearly to $R_{\text{clog}} = 0.3$. The prediction (5.16) gives $T_{\text{end}} = 7.5$ for the parameter values used in figure 6b, which is seen to be fairly accurate, although a slight underestimate, as this does not take into account the early time (in $\tilde{T}$, or $O(1)$ in T) stage.

The dry-clogging that we have described in this section always occurs for $\kappa \ll 1$, but it may also occur for $\kappa = O(1)$, when the deposition rate is on the same order as the evaporation rate. Indeed, the model (2.20) must *always* dry-clog for $\kappa > 0$, even if $\beta = 0$. This is because, if $\beta = 0$, θ can never reach zero even for large κ, and can only decay exponentially towards it. However, if $\kappa \gg 1$ is sufficiently large that θ is very close to zero by the end stages of the drying, the dry-clogging occurs at a negligible distance from the end of the domain, $H = 1$, and is not physically meaningful. We discuss this more in section 7 below. Furthermore, if $\beta > 0$ then we expect $\theta \geqslant \beta$ for all time (so long as this is true initially). In this case we would certainly anticipate much more prominent dry-clogging behaviour, for a wider range of parameters, although to investigate this thoroughly is beyond the scope of the present study.

6. The fast deposition limit ($\kappa \gg 1$) and wet-clogging

We now consider the limit of $\kappa \gg 1$, in which the deposition of dirt occurs much faster than the motion of the evaporation front. Since the deposited dirt layer grows quickly, it can become large enough to significantly affect the effective diffusivity $\mathcal{D}$ and porosity ϕ, if θ_{IC} is sufficiently large, impacting on the drying dynamics. In particular, the deposited dirt layer thickness R may reach the maximum radius $R_{\text{clog}} = 1/2 - r_0$, at which the diffusivity $\mathcal{D} = 0$, and the system is clogged early in the domain, when θ is not $\hat{\theta}$ in $Y > H(T)$, so that a non-negligible quantity of liquid is trapped by the clogging. We refer to this type of clogging as "wet-clogging" as, compared with the dry-clogging behaviour discussed in section 5.2, a non-negligible amount of liquid is trapped by the clogging. This wet-clogging mechanism is illustrated in figure 5 (right).

6.1. *Large κ behaviour*

To understand the deposition (and potential clogging) behaviour when $\kappa \gg 1$, we change to the fast timescale over which R varies, by setting

$$T = \frac{1}{\kappa}\bar{t}, \tag{6.1}$$

where $\bar{t} = O(1)$. At such early times the evaporating interface is close to the surface of the porous material, and we rescale

$$H = \frac{1}{\sqrt{\sigma\kappa}}\bar{h}, \quad Y = \frac{1}{\sqrt{\sigma\kappa}}\bar{y}, \tag{6.2}$$

for $Y < H(T)$, (assuming that $\sigma\kappa \gg 1$) so that (3.3) becomes

$$\frac{1}{\sigma}\bar{h}_{\bar{t}} \int_0^{\bar{h}} \frac{1}{\mathcal{D}(R(\bar{y}))}\,\mathrm{d}\bar{y} = -\frac{1}{\nu\phi|_{\bar{h}}} \log\left(\frac{1-\nu f(\theta|_h)}{1-\nu\alpha}\right). \tag{6.3}$$

For $Y > H = (1/\sqrt{\sigma\kappa})\bar{h}$, we see that (2.20*b*)–(2.20*c*) become

$$\phi\theta_{\bar{t}} = \frac{1}{\sigma\kappa}\left(\mathcal{D}\theta_Y\right)_Y - C(\theta_* - \theta)(\theta - \beta\chi_R), \tag{6.4}$$

$$R_{\bar{t}} = \theta - \beta\chi_R. \tag{6.5}$$

To leading order in $(\kappa\sigma)^{-1} \ll 1$, we have a plane-autonomous deposition system:

$$\phi(R)\theta_{\bar{t}} = -C(R)(\theta_* - \theta)(\theta - \beta\chi_R), \tag{6.6a}$$

$$R_{\bar{t}} = \theta - \beta\chi_R. \tag{6.6b}$$

We refer to the system (6.6) as the *outer problem*, which holds away from the evaporation front in the majority of the domain. (At the evaporation front there must be a boundary layer, which we will discuss later.) Specifically, the initial conditions $\theta = \theta_{IC} > \beta$ and $R = 0$ at $\bar{t} = 0$, imply that both θ and R are independent of Y for all $\bar{t}$, and, recalling that $\phi(R) = 1 - \pi(r_0 + R)^2$ and $C(R) = -\phi'(R) = 2\pi(r_0 + R)$, a first integral from (6.6) is

$$\phi(R)(\theta_* - \theta) = \phi(0)(\theta_* - \theta_{IC}), \tag{6.7}$$

which is independent of time $\bar{t}$. This equation (6.7) may be interpreted as an expression of overall conservation of dirt: since there is no transport of dirt on this timescale, the total suspended dirt in the liquid and deposited dirt in the layer, must remain constant in time. We could use (6.7) in (6.6) to find implicit expressions for the spatially uniform R and θ, although this is not particularly illustrative. Instead, we use (6.7) to plot the phase plane in the outer region in figure 7. The system begins at $R = 0$, $\theta = \theta_{IC}$. If $\theta_{IC} > \beta$ we see from (6.6*b*) that R increases in time and, from (6.7), that θ decreases towards $\theta = \beta$. If instead $\theta_{IC} \leqslant \beta$, then R remains zero and θ remains at its initial value (as any deposited dirt immediately re-suspends, from (6.6*b*)). We note that the system clogs if R reaches R_{clog} before θ reaches β. We see that this occurs for sufficiently large initial suspended dirt concentrations, namely (from (6.7)) if

$$\theta_{IC} > \theta_{IC}^{\mathrm{crit}} := \theta_* - (\theta_* - \beta)\left(\frac{1-\pi/4}{1-\pi r_0^2}\right). \tag{6.8}$$

Although this analysis shows that the system certainly clogs for $\theta_{IC} > \theta_{IC}^{\mathrm{crit}}$ (in this limit $\kappa\sigma \gg 1$), we expect that the system will in fact clog for lower values of θ_{IC} too, since we expect there will be higher θ and therefore faster deposition near to the evaporation front at $\bar{h}$.

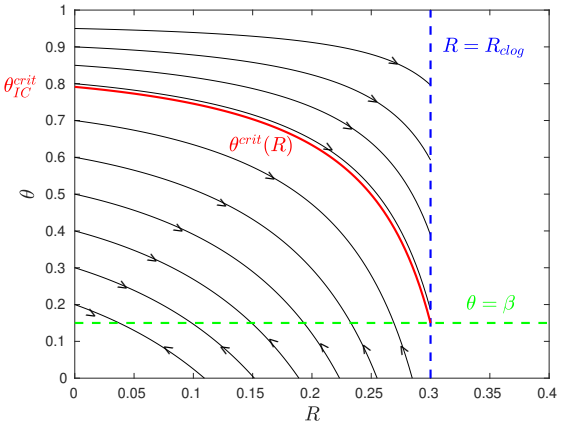

Figure 7: Phase plane dynamics in the outer region when $\kappa \gg 1$. Black curves show trajectories, with the system moving down these curves from $(0, \theta_{IC})$ to the attractor at $\theta = \beta$ (direction shown by arrows). For $\theta_{IC} > \theta_{IC}^{\text{crit}}$, the trajectory hits $R = R_{\text{clog}}$ before reaching $\theta = \beta$. Here we take $\theta_* = 1$, $\beta = 0.15$, $r_0 = 0.2$.

Indeed, in a boundary layer of width $O(1/\sqrt{\sigma\kappa})$, dirt accumulates due to the motion of the evaporation front. By making the change of variables

$$Y = \frac{1}{\sqrt{\sigma\kappa}}\left(\bar{h} + z\right), \tag{6.9}$$

we find that, in the boundary layer $z \in (0, \infty)$,

$$\phi\left(\theta_{\bar{t}} - \bar{h}_{\bar{t}}\theta_z\right) = \left(\mathcal{D}\theta_z\right)_z - C(\theta_* - \theta)(\theta - \beta\chi_R), \tag{6.10a}$$

$$R_{\bar{t}} - \bar{h}_{\bar{t}}R_z = \theta - \beta\chi_R, \tag{6.10b}$$

while at the evaporation interface $z = 0$,

$$\phi\theta\bar{h}_{\bar{t}} + \mathcal{D}\theta_z = 0, \tag{6.10c}$$

and, as $z \to \infty$,

$$R \to R^{\text{out}}(\bar{t}), \qquad \theta \to \theta^{\text{out}}(\bar{t}), \tag{6.10d}$$

where R^{out} and θ^{out} are the values in the outer region, as described above. This boundary layer system (6.10), coupled with (6.3), describes the motion of the evaporation front, accumulation of suspended dirt ahead of it, and the deposition of dirt. We note that dirt accumulation, transport, and deposition all balance in the boundary layer.

We show a solution with $\kappa = 100$ in figure 8. The subplots 8a–d show the spatial profiles for ρ, θ and R at four successive times, while the motion of the evaporation front $H(T)$ is shown in figure 8e, with the time-points of the plots a–d marked as red circles. At early times, in 8a and b, we clearly see the boundary layer structure in the θ and R plots in $Y > H$, with both R and θ uniform in the rest of the domain. As time progresses, we see that R increases while θ decreases, as suspended dirt becomes deposited onto the solid structure. By the time shown in figure 8c, we see that θ is close to zero everywhere: the deposition has nearly finished. Since $\kappa \gg 1$ this occurs when the evaporation front is still only a short $O(\sqrt{\kappa})$ distance into the domain. After this time, $\theta(\approx 0)$ and R are both constant in $Y > H$, and the evaporation front travels to the bottom of the domain, resulting in a fully dry porous material with non-uniformly deposited dirt. Indeed we note that the combination of dirt accumulation,

diffusion, and deposition in the boundary layer, results in an internal spatial peak in the final thickness, R, of the deposited dirt layer (for $Y < H$) near the top of the domain. Since R is higher here, the effective diffusivity of the vapour is correspondingly reduced. This can be seen in the non-monotone gradient of ρ in figure 8d, where the ρ-profile is steepest at the peak value of R. The reduced diffusivity here limits the drying rate for the remainder of the process.

The fact that we obtain this internal peak in R at early time due to the boundary layer accumulation, diffusion, and deposition of dirt, means that our estimate for the clogging criterion (6.8), which assumes that dirt deposits in a spatially uniform way, must be an upper bound on the true critical θ_{IC}: we expect to have clogging at θ_{IC} lower than the critical value given by (6.8). Indeed, in figure 9 we show a simulation for the same parameter values as in figure 8, except that we take a larger initial suspended dirt volume fraction $\theta_{IC} = 0.6$ which is still lower than the estimate of $\theta_{IC}^{\text{crit}} = 0.755$ given by (6.8), for the chosen parameter values. Nevertheless, we see that the system indeed clogs early in the domain. Both liquid and suspended dirt are trapped ahead of the clogged point, since $\theta < 1$ in $Y > H$. The clogging happens at an $O(1/\sqrt{\kappa})$ distance into the domain, at $H \approx 0.07$, and after an $O(1/\kappa)$ time, as predicted by our analysis above.

We notice that the motion of the evaporation front shown in figure 9b no longer follows a $\sqrt{T}$ behaviour. Instead we see that the speed H_T of the evaporation front is not smoothly decreasing. Evaporation is fast to start with as R is small and the vapour has only a short way to travel to the surface of the porous material. Then the evaporation front begins to slow down, as both $\theta|_H$ increases due to accumulation and the effective diffusivity $\mathcal{D}$ decreases, as R begins to increase. As the clogging point is approached, H_T increases again, because the porosity ϕ is decreasing, so that there is less liquid in the pore-space to be evaporated since so much of the pore-space is occupied by the deposited and suspended dirt. Similar time-varying behaviour of H_T is visible at early times in the case shown in figure 8e (inset), when the system did *not* clog.

Evidently, wet-clogging can occur at initial suspended dirt volume fractions θ_{IC} significantly below the estimate for the critical value given by (6.8). To better understand the clogging criterion we must better understand the behaviour in the boundary layer at $Y = H$. However, the non-linearity of the boundary layer equations (6.10) makes them intractable to further analytical progress. Instead, we study a paradigm problem in the next section, which is a simplified version of the large-κ problem, but which still captures the essence of the wet-clogging behaviour.

6.2. *The clogging criterion for a paradigm problem*

In section 6.1 we saw numerically that, for large κ, the deposited dirt layer thickness R is non-uniform near $Y = 0$, increasing from zero to $R_{\max} := \max_T(R|_H)$ that is larger than the final value of R attained in the outer-region. This means that wet-clogging occurs for lower values of θ_{IC} than predicted by the outer-region estimate (6.8). Since the spatially uniform deposition dynamics in the outer region do not capture this non-uniformity in R near to $Y = 0$, we would like to consider the behaviour in the boundary layer at $Y = 0$, where there is a balance between all of accumulation, diffusion, and deposition of dirt, in order to derive an improved criterion for wet-clogging.

However, the boundary-layer equations (6.10) are intractable analytically, due to the coupling between variables and the nonlinear terms. In order to build intuition for what determines the size of the peak $R_{\max}$, in this section we investigate a paradigm problem, with a different functional form for $f(\theta)$, and unphysical simplifications of $\mathcal{D}$ and the bulk deposition term. With these (non-systematic) simplifications, we solve the boundary-layer

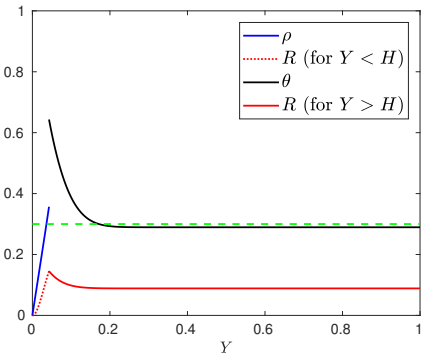

(a) $T = 0.0025$

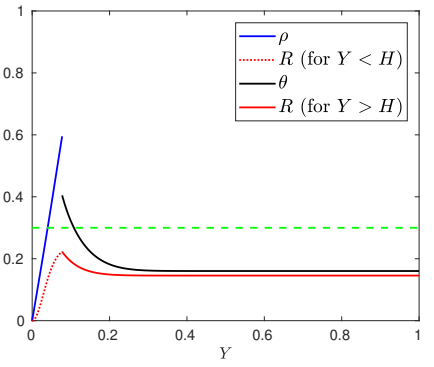

(b) $T = 0.005$

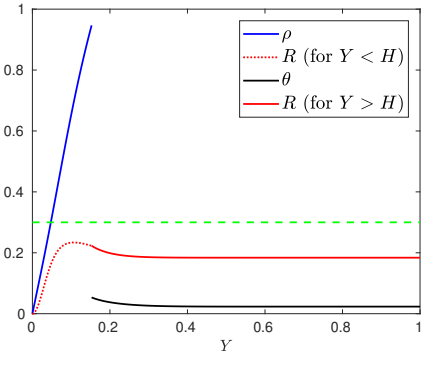

(c) $T = 0.01$

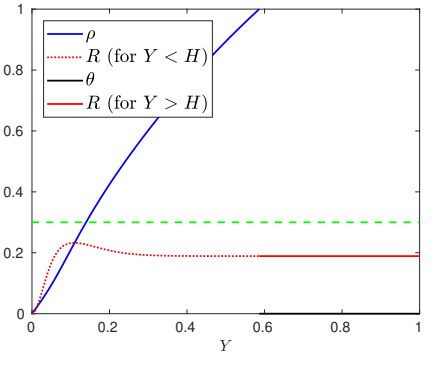

(d) $T = 0.1$

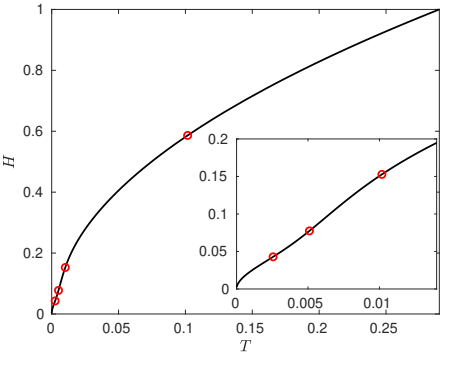

(e) Motion of the evaporation front

Figure 8: Numerical solution of (2.20) for large deposition rate $\kappa = 100$. We also take $f(\theta) = 1 - \theta$, $\alpha = 0$, $\beta = 0$, $\nu = 0.5$, $\sigma = 1$, $\theta_{IC} = 0.4$, $\delta = 10^{-3}$ and $r_0 = 0.2$. The green-dashed line in figures a–d shows the clogging point, $R_{\text{clog}} = 0.5 - r_0$, which is not attained in this simulation.

equations (6.10) explicitly, and hence determine $R_{\max}$ analytically. In this way, we determine a criterion for wet clogging (given by $R_{\max} \geqslant R_{\text{clog}}$), and build intuition for the more general case.

We assume for simplicity that $\beta = 0$ and $\alpha = 0$. Additionally, we suppose that r_0 is close to $1/2$, so that $R \ll r_0$ (since the circular inclusions are close together, and only thin deposited-

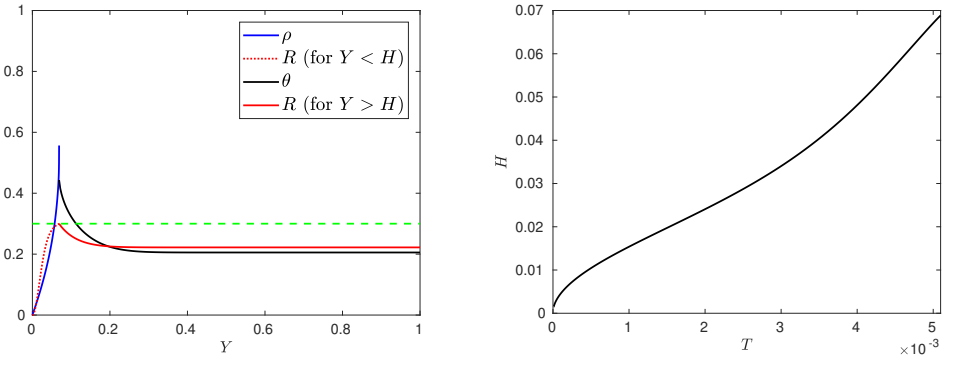

(a) (b)

Figure 9: Wet-clogging: numerical solution of (2.20) for large deposition rate $\kappa = 100$ and $\theta_{IC} = 0.6$. We also take $f(\theta) = 1-\theta$, $\alpha = 0$, $\beta = 0$, $\sigma = 1$, $\nu = 0.5$, $\delta = 10^{-3}$ and $r_0 = 0.2$. The green-dashed line shows the clogging point, $R_{\text{clog}} = 0.5 - r_0$, which is attained at $T \approx 5.1 \times 10^{-3}$ in this simulation. The profiles in (a) are at the time when the system clogs with $R = R_{\text{clog}}$ at $Y = H$.

dirt layers are possible before clogging occurs). Then $\phi \approx \phi_0$ and $C \approx C_0$ are approximately constant, even for R approaching R_{clog}. We make the additional approximations

$$\mathcal{D} = \begin{cases} \mathcal{D}_0 & \text{if } R < R_{\text{clog}}, \\ 0 & \text{if } R = R_{\text{clog}}, \end{cases} \qquad f(\theta) = \begin{cases} 1 & \text{if } \theta < 1, \\ 0 & \text{if } \theta = 1. \end{cases} \tag{6.11}$$

Finally, we alter the deposition term in (6.10) by replacing the factor $\theta_* - \theta$ with the constant value θ_*. With these choices of functional forms (which we emphasise are not a true limit of the full problem), the paradigm boundary layer problem is, while $\theta < 1$,

$$\frac{1}{\sigma \mathcal{D}_0} \bar{h} \bar{h}_{\bar{t}} = -\frac{1}{\nu \phi_0} \log(1-\nu), \tag{6.12a}$$

along with, in $z \in (0, \infty)$ and while $R < R_{\text{clog}}$,

$$\phi_0 \left(\theta_{\bar{t}} - \bar{h}_{\bar{t}} \theta_z \right) = \mathcal{D}_0 \theta_{zz} - C_0 \theta_* \theta, \tag{6.12b}$$

$$R_{\bar{t}} - \bar{h}_{\bar{t}} R_z = \theta, \tag{6.12c}$$

while at the evaporation interface $z = 0$,

$$\phi_0 \theta \bar{h}_{\bar{t}} + \mathcal{D}_0 \theta_z = 0, \tag{6.12d}$$

and, as $z \to \infty$,

$$R \to R^{\text{out}}(\bar{t}), \qquad \theta \to \theta^{\text{out}}(\bar{t}), \tag{6.12e}$$

where the outer solution R^{out}, θ^{out} satisfy

$$\phi_0 \theta^{\text{out}}_{\bar{t}} = -C_0 \theta_* \theta^{\text{out}}, \tag{6.12f}$$

$$R^{\text{out}}_{\bar{t}} = \theta^{\text{out}}. \tag{6.12g}$$

Initially, at $\bar{t} = 0$,

$$\theta = \theta_{IC}, \qquad R = 0, \qquad \bar{h} = 0. \tag{6.12h}$$

Solving (6.12), we see from (6.12*a*) that the evaporation front is simply

$$\bar{h} = B\sqrt{D\bar{t}}, \tag{6.13}$$

where, for simplicity of notation, we define

$$B := \sqrt{-\frac{2\sigma}{\nu}\log(1-\nu)}, \qquad D := \frac{\mathcal{D}_0}{\phi_0}. \tag{6.14}$$

Furthermore, the outer region phase-plane equations (6.12*f*)–(6.12*g*) decouple, with explicit solution

$$\theta^{\text{out}} = \theta_{IC}\exp\left(-C\bar{t}\right), \quad R^{\text{out}} = \frac{\theta_{IC}}{C}\left(1-\exp\left(-C\bar{t}\right)\right), \tag{6.15}$$

where, again for simplicity of notation, we define

$$C := \frac{C_0\theta_*}{\phi_0}. \tag{6.16}$$

The boundary layer equations (6.12*b*)–(6.12*e*) are therefore

$$\theta_{\bar{t}} - \frac{B\sqrt{D}}{\sqrt{\bar{t}}}\theta_z = D\theta_{zz} - C\theta, \qquad R_{\bar{t}} - \frac{B\sqrt{D}}{\sqrt{\bar{t}}}R_z = \theta, \tag{6.17a}$$

while, at the evaporation interface $z = 0$,

$$\frac{B\sqrt{D}}{\sqrt{\bar{t}}}\theta + D\theta_z = 0, \tag{6.17b}$$

and, as $z \to \infty$,

$$\theta \to \theta_{IC}\exp\left(-C\bar{t}\right), \qquad R \to \frac{\theta_{IC}}{C}\left(1-\exp\left(-C\bar{t}\right)\right). \tag{6.17c}$$

Thus, under all of our simplifying assumptions, the equations for θ and R decouple: we may solve the linear system (6.17*a*) (left), (6.17*b*) and (6.17*c*) (left) for θ, before then computing R.

Specifically, we look for a solution for θ of the form

$$\theta = \theta_{IC}e^{-C\bar{t}}F(\eta), \quad \text{where} \quad \eta = \frac{z}{\sqrt{D\bar{t}}} \tag{6.18}$$

is a similarity variable. Thus in the boundary layer the far-field deposition solution $\theta^{\text{out}} = \theta_{IC}e^{-C\bar{t}}$ is modified by an "accumulation factor" F, which describes how the evaporation causes suspended dirt to accumulate near the evaporating interface. Substituting this form of θ into (6.17*a*) (left), (6.17*b*) and (6.17*c*) (left), and solving the resulting ODE system for $F(\eta)$, we find

$$\theta = \theta_{IC}e^{-C\bar{t}}\left(1 + \frac{\sqrt{\pi}Be^{B^2}}{1-\sqrt{\pi}Be^{B^2}\text{erfc}(B)}\text{erfc}\left(B + \frac{z}{2\sqrt{D\bar{t}}}\right)\right). \tag{6.19}$$

The factor $1 - \sqrt{\pi}Be^{B^2}\text{erfc}(B)$ is always positive (although it approaches zero as B, or equivalently σ, approaches ∞), and so the accumulation factor $F > 1$ (and $F \to 1$ as η (or z)$\to \infty$). Thus, as we would expect, the value of θ is higher in the boundary layer than in the far-field.

The large θ in the boundary layer results in greater deposition occurring there, and so R increases compared with the solution as $z \to \infty$. The problem (6.17*a*) (right) for R is

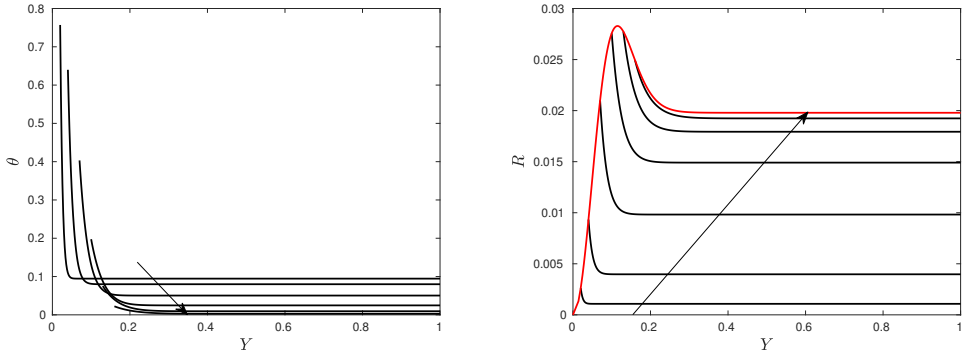

(a) (b)

Figure 10: The black curves are the analytic solution (a) θ given by (6.19) and (b) R for $Y > H$ given by (6.20), of the paradigm problem (6.17), at various times through the drying, with arrows showing increasing time. The red curve in (b) shows the final deposited dirt layer after the drying is completed. We have taken parameter values $\kappa = 100$, $\nu = 0.5$, $\sigma = 1$, $\theta_{IC} = 0.1$, and $r_0 = 0.4$.

first order hyberbolic, and — given the form (6.19) — may be solved using the method of characteristics. Specifically, we find the characteristic curves take the form $z = z_0 - 2B\sqrt{D\bar{t}}$, where z_0 parameterises the initial data $R = 0$ at $\bar{t} = 0$. (The shape of the characteristic curves mean we do not require data for R at $\bar{z} = 0$.) The solution R, in terms of z and $\bar{t}$, is given by

$$\begin{aligned} R(z,\bar{t}) =& \frac{\theta_{IC}}{C}\left(1 - e^{-C\bar{t}}\right) \\ &+ \frac{\theta_{IC}\sqrt{\pi}Be^{B^2}}{2C(1-\sqrt{\pi}Be^{B^2}\mathrm{erfc}(B))}\left[e^{-(\sqrt{C/D}z+2B\sqrt{C\bar{t}})}\mathrm{erfc}\left(\frac{z}{2\sqrt{D\bar{t}}} + B - \sqrt{C\bar{t}}\right)\right. \\ &\left. + e^{(\sqrt{C/D}z+2B\sqrt{C\bar{t}})}\mathrm{erfc}\left(\frac{z}{2\sqrt{D\bar{t}}} + B + \sqrt{C\bar{t}}\right) - 2e^{-C\bar{t}}\mathrm{erfc}\left(\frac{z}{2\sqrt{D\bar{t}}} + B\right)\right]. \end{aligned} \tag{6.20}$$

The solutions (6.19) and (6.20) of the paradigm model (6.17) are shown in figure 10. Clearly the system bears qualitative resemblance to the full model. The deposited dirt layer thickness is maximised (spatially in the liquid–dirt domain, at any given time) at the evaporation front. Evaluating (6.20) at $z = 0$, we have

$$\begin{aligned} R|_{\bar{h}} =& \frac{\theta_{IC}}{C}\left(1 - e^{-C\bar{t}}\right) + \frac{\theta_{IC}\sqrt{\pi}Be^{B^2}}{2C(1-\sqrt{\pi}Be^{B^2}\mathrm{erfc}(B))}\times \\ &\left[e^{-2B\sqrt{C\bar{t}}}\mathrm{erfc}\left(B - \sqrt{C\bar{t}}\right) - 2e^{-C\bar{t}}\mathrm{erfc}\,(B) + e^{2B\sqrt{C\bar{t}}}\mathrm{erfc}\left(B + \sqrt{C\bar{t}}\right)\right] \end{aligned} \tag{6.21}$$

In order to find the maximum value R attains, we simply maximise $R|_{\bar{h}}$ over $\bar{t}$. We find that there is a single maximum for positive $\bar{t}$, at the critical time $\bar{t}_* = \tau_*^2/C$, where $\tau_* = \tau_*(B)$ satisfies

$$\frac{2\tau_*}{\sqrt{\pi}B^2} = e^{(B-\tau_*)^2}\mathrm{erfc}(B - \tau_*) - e^{(B+\tau_*)^2}\mathrm{erfc}(B + \tau_*). \tag{6.22}$$

The solution τ_* of (6.22) is shown as a function of B in figure 11 (left). We see $O(1)$ variation of τ_* when B varies over 6 orders of magnitude. Indeed $\tau_* \to \sqrt{3/2}$ as $B \to \infty$ (or $\sigma \to \infty$,

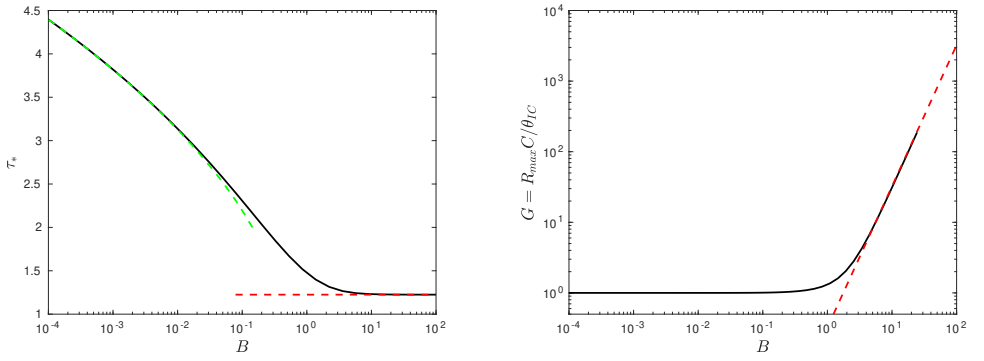

(a) (b)

Figure 11: The maximum of R for the paradigm problem. (a): the solution τ_* of (6.22) as a function of B, with the large B limit $\sqrt{3/2}$ (red dashed) and the small-B limit, namely the (non-negligible) root of $\tau_* e^{-\tau_*^2} = \sqrt{\pi}B^2$ (green dashed). (b): The (scaled) maximum value of $R_{\max}$, given by (6.25), against B. For small B we have $G \sim 1$ while for large B we have $G \sim e^{-3/2}(\sqrt{6}-1)B^2$ (red dashed).

say, the limit of slow dirt diffusion), whilst τ_* grows very slowly as $B \to 0$, behaving like the growing root of $\tau_* e^{-\tau_*^2} = \sqrt{\pi}B^2$ for $B \ll 1$, namely

$$\tau_* \sim \sqrt{\frac{-W_{-1}(-2\pi B^4)}{2}} \sim \sqrt{\log\left(\frac{1}{\sqrt{\pi}B^2}\right)} + \frac{\log\left(\log\left(\frac{1}{\sqrt{\pi}B^2}\right)\right)}{\sqrt{\log\left(\frac{1}{\sqrt{\pi}B^2}\right)}} + \ldots, \tag{6.23}$$

where W_{-1} is the lower branch of the real Lambert W function.

From the critical time $\bar{t}_*$, we can compute the value that R attains at its maximum, namely

$$R_{\max} = \frac{\theta_{IC}}{C} G(B), \tag{6.24}$$

where

$$G(B) = 1 + \frac{1}{1 - \sqrt{\pi}Be^{B^2}\mathrm{erfc}(B)}\left(e^{-\tau_*^2}(\tau_* - 1) + \frac{\sqrt{\pi}Be^{B^2}}{2} e^{2B\tau_*}\mathrm{erfc}(B + \tau_*)\right), \tag{6.25}$$

with τ_* the solution of (6.22). We show $G = R_{\max}C/\theta_{IC}$ as a function of B in figure 11 (right). For $B \ll 1$ we see from (6.25) that $G \approx 1$, while for $B \gg 1$ we find, using the large-B value $\tau_* \approx \sqrt{3/2}$, along with the facts that $1 - \sqrt{\pi}Be^{B^2}\mathrm{erfc}(B) \sim 1/(2B^2)$ and $\sqrt{\pi}Be^{B^2}e^{\sqrt{6}B}\mathrm{erfc}(B + \sqrt{3/2}) \to e^{-3/2}$ as $B \to \infty$, that

$$G \sim e^{-3/2}\left(\sqrt{6} - 1\right)B^2 \qquad \text{as } B \to \infty. \tag{6.26}$$

We note from (6.14) that $B = O(\sqrt{\sigma})$, and so $R_{\max}$ and G increase linearly with σ as $\sigma \to \infty$. Thus we see that, no matter how small the initial suspended dirt level θ_{IC}, for sufficiently slow dirt diffusion (sufficiently large σ) we will find that $R_{\max}$ exceeds R_{clog} and the system will clog.

Indeed, this expression (6.24) for $R_{\max}$ gives the clogging condition for this paradigm

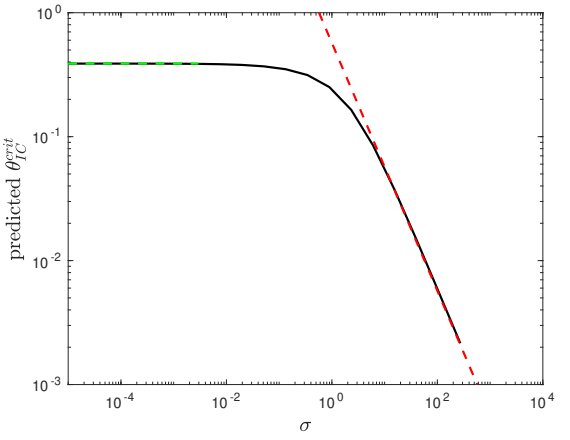

Figure 12: The critical initial suspended dirt volume fraction (6.27) predicted in the paradigm case, as a function of σ. Dashed curves are the low and high σ limits (6.28). We take parameter values $r_0 = 0.45$, $\nu = 0.1$, and $\theta_* = 1$.

setting: the system clogs when $R_{\max} \geqslant R_{\text{clog}}$. Using (6.16), this clogging criterion is

$$\theta_{IC} \geqslant \theta_{IC}^{\text{crit}} := \frac{C_0 \theta_* R_{\text{clog}}}{\phi_0 G(B(\sigma, \nu))}. \tag{6.27}$$

We show this critical initial suspended dirt volume fraction (6.27) as a function of the suspended dirt diffusion rate σ in figure 12, along with the small and large σ limits (which follow directly from the small and large B behaviour of G discussed above), namely

$$\theta_{IC}^{\text{crit}} \to \frac{C_0 \theta_* R_{\text{clog}}}{\phi_0} \qquad \text{as } \sigma \to 0, \tag{6.28a}$$

$$\theta_{IC}^{\text{crit}} \to \frac{e^{3/2} \nu C_0 \theta_* R_{\text{clog}}}{2\phi_0(\sqrt{6}-1)\log(1/(1-\nu))} \sigma^{-1} \qquad \text{as } \sigma \to \infty. \tag{6.28b}$$

We note that, since $G \geqslant 1$ and $R_{\text{clog}} > 0$ this $\theta_{IC}^{\text{crit}}$, given by (6.27), for the paradigm problem is strictly smaller than the upper bound (6.8) (that essentially assumes a uniform deposited dirt layer), since, in the case $\beta = 0$ that we have assumed for the paradigm case, the upper bound (6.8) may be rearranged to be written in terms of $\phi_0 = 1 - \pi r_0^2$, $C_0 = 2\pi r_0$ and $R_{\text{clog}} = 1/2 - r_0$, becoming

$$\theta_{IC}^{\text{crit}} = \frac{\theta_*(C_0 R_{\text{clog}} + \pi R_{\text{clog}}^2)}{\phi_0}. \tag{6.29}$$

Thus, as expected, the non-uniformity of the dirt deposit in the boundary layer at the evaporation front results in clogging for lower initial suspended dirt volume fractions than if the dirt were to deposit uniformly.

We note that our expression (6.27) for $\theta_{IC}^{\text{crit}}$ in this paradigm case is independent of κ, since we have taken the leading-order behaviour as $\kappa \to \infty$. Since we require the boundary layer structure, our paradigm estimate for the clogging criterion is only valid when the width $1/\sqrt{\sigma\kappa}$ of the boundary layer is small, and so only for σ sufficiently large that $\sigma \gg 1/\kappa$ (although since we assume $\kappa \gg 1$ this is not particularly restrictive).

Additionally, we see that the expression (6.27) is independent of D, and hence of $\mathcal{D}_0$. From this, we learn that it is the relative diffusivity of the suspended dirt and the liquid vapour,

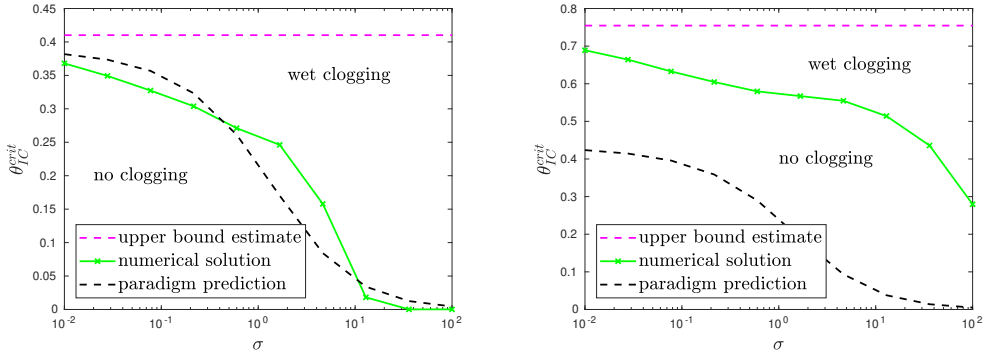

(a) (b)

Figure 13: The numerically computed critical initial suspended dirt volume fraction $\theta_{IC}^{\text{crit}}$, in the case of large $\kappa = 100$, and with (a) $r_0 = 0.45$ and (b) $r_0 = 0.2$. We also show the upper bound, (6.8), and the prediction of the paradigm model, (6.27), for $\theta_{IC}^{\text{crit}}$. Throughout the figure we take $f = 1 - \theta$, $\alpha = 0$, $\beta = 0$, and $\nu = 0.5$, and use $\delta = 10^{-3}$ for the numerical simulation.

captured through σ that is important, and not how both are equally affected by the presence of the porous material (recall that $\mathcal{D}_0$ is the effective diffusivity). Of course, the depth y into the porous material at which the clogging occurs *does* depend on D. Specifically, the clogging depth when $\theta_{IC} = \theta_{IC}^{\text{crit}}$ takes its critical value is

$$H_{\text{clog}}^{\text{crit}} = \sqrt{\frac{2\mathcal{D}_0 \log(1/(1-\nu))}{\nu C_0 \theta_*}} \frac{\tau_*}{\sqrt{\kappa}} \tag{6.30}$$

Curiously, although this position given by (6.30) depends on κ and $\mathcal{D}_0$, it is only weakly dependent on σ, since τ_* (the solution of (6.22)) was seen to have very weak dependence on $B \propto \sqrt{\sigma}$.

We have considered a simplified, paradigm version of the problem in this section, in order to make analytic progress. Although this analysis does not directly relate to the full drying model, we may extrapolate some general conclusions. Firstly, the qualitative wet-clogging behaviour seen in the full model, characterised by an internal peak in R, does not rely on the variation of $\mathcal{D}$, ϕ, and the evaporation front speed h_T with R and θ (in the paradigm case we supposed all these were constant). Instead, the important mechanism, captured by the paradigm model, is the variation of the rate of dirt deposition with θ, along the fact that θ is spatially non-uniform in the boundary layer at the evaporation front, determined by a balance of all three mechanisms of diffusion, accumulation due to liquid evaporation, and the deposition.

In the following section we generate bifurcation diagrams showing parameter regimes for which the system clogs. We will compare these numerical results with the predictions of the paradigm model as appropriate.

7. Clogging parameter regimes

Having built understanding of the two mechanisms by which the porous material may clog, in this section we compute bifurcation diagrams numerically in order to quantify the parameter regimes for which clogging occurs.

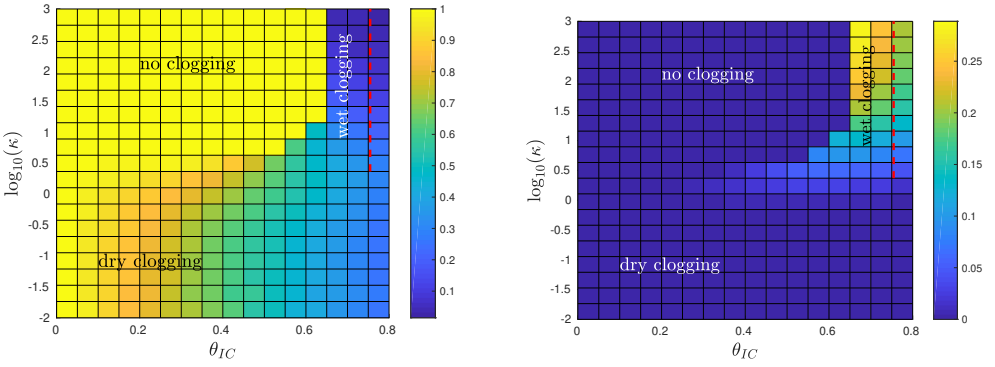

Figure 14: Clogging behaviour of (2.20) as κ is varied. (a): The end position H_{end} when the evaporation terminates, so $H_{\text{end}} = 1$ if the drying is complete without clogging, $H_{\text{end}} < 1$ indicates clogging. (b): the total volume of liquid remaining in the porespace when the evaporation terminates. On both (a) and (b), the red dashed line indicates the upper estimate (6.8) for the wet-clogging criterion. Throughout the figure we take $\sigma = 0.1$, $f = 1 - \theta$, $\alpha = 0$, $\beta = 0$, and $\nu = 0.5$, $r_0 = 0.2$ and $\delta = 10^{-3}$.

Firstly, we consider the case $\kappa \gg 1$ for which the dirt deposition rate is high relative to the evaporation rate. As in section 6, we do not expect the system to dry-clog, but instead to exhibit wet-clogging for sufficiently large θ_{IC} and σ. In figure 13a and b we show the numerically computed regions of parameter space for which dry-clogging occurs, for two different values of the microscale-geometry parameter r_0. For both, we observe that there is a well-defined critical suspended dirt volume fraction $\theta_{IC}^{\text{crit}}$ above which the system clogs, and below which there is no clogging and the evaporation front reaches $H = 1$. We see that $\theta_{IC}^{\text{crit}}$ is a monotone decreasing function of σ. The estimate (6.8) is indeed seen to be an upper bound for the numerically computed $\theta_{IC}^{\text{crit}}$, and is most accurate for small σ, when the diffusion of dirt is fast and so dirt deposition is approximately uniform. For $r_0 = 0.45$ (figure 13a), where $R_{\text{clog}} = 0.05$ is fairly small and ϕ and C do not vary much with R, we see that the prediction (6.27) of the paradigm model is, in fact, a reasonable approximation for the full system, despite the fact that the paradigm model is not a real limit of the full model. In particular, for large σ we observe wet-clogging for very small initial suspended dirt volume fractions. For $r_0 = 0.2$ (figure 13b), the paradigm model prediction of $\theta_{IC}^{\text{crit}}$ is a poor approximation of the full system.

In figure 14 we investigate the effect of the deposition rate κ and the initial condition θ_{IC} on the clogging behaviour. We simulate the model (2.20) for each set of parameter values (θ_{IC}, κ), and in figure 14a the colour indicates the position H_{end} of the evaporating interface at the time when the simulation terminated (so $H_{\text{end}} = 1$ if there was no clogging and the evaporation completed, while $H_{\text{end}} < 1$ if the system clogged). In figure 14b, for the same set of model simulations, the colour indicates the volume of liquid remaining when the simulation terminates, namely

$$\text{liquid volume remaining} = \int_{Y=H_{\text{end}}}^{1} \phi(1-\theta)\,\mathrm{d}Y. \tag{7.1}$$

We note that the κ-axis is on a log-scale in figure 14. For large κ we see that there is a critical $\theta_{IC} \approx 0.65$, which appears to be largely independent of κ, above which we have wet-clogging and below which the system does not clog. A non-negligible amount of

liquid remains trapped in the porespace when the evaporation terminates. This wet-clogging behaviour is as discussed in section 6. The upper bound on the critical initial suspended dirt volume fraction $\theta_{IC}^{\text{crit}}$, given by (6.8) and shown by the red-dashed curve, is seen to be a significant overestimate, even for the relatively small value $\sigma = 0.1$ (as in figure 13 we expect (6.8) to be most accurate for small σ). We see that, as κ increases, the wet-clogging occurs earlier (H_{end} is smaller) and correspondingly more liquid remains trapped in the porespace.

For small κ, we observe dry-clogging behaviour, as discussed in section 5, with $H_{\text{end}} < 1$ but with a negligible amount of liquid trapped in the porespace, since $\theta \approx 1$ for $Y > H$ in this case. For $\kappa \ll 1$ we see that dry-clogging occurs for all $\theta_{IC} > 0$, to varying degrees, with H_{end} close to one for small θ_{IC}, but actually very small for larger values of θ_{IC}. The transition from the no-clogging/wet-clogging regime for $\kappa \gg 1$ to the dry-clogging for $\kappa \ll 1$ is gradual. Indeed, for $\kappa = O(1)$, for which we were unable to make analytic progress, it is not clear how to classify the system. For small θ_{IC} there is some dry-clogging, with $H_{\text{end}} \approx 1$ and the remaining liquid volume very small. Moreover, for larger θ_{IC} the behaviour could be considered to be either dry- or wet-clogging, with H_{end} around halfway through the domain, and a fairly small amount of liquid remaining trapped in the pore space.

8. Discussion and Conclusions

We have derived and analysed a model for the drying of liquid from within a porous material and the associated deposition of impurities within the pore structure. By beginning with a pore-scale model and systematically homogenising, we have incorporated delicate couplings between the dependent variables, including the effect of a growing layer of deposited dirt on the porosity, the diffusivity of both dirt and vapour, and on the deposition rate of the dirt. We explored the relevant limit where the vapour density is much smaller than the liquid density ($\delta \ll 1$); in this case, the vapour-transport problem was reduced to a single equation for the motion of the evaporation front. Our resulting equation is valid in the physically-relevant limit where the vapour transport through the porous material limits the evaporation. This is different to prescribing an evaporation rate, which a common approach in the literature, and which is only valid when the vaporisation of the liquid molecules is the limiting mechanism.

The accumulation of suspended dirt at the evaporating interface during drying was shown to reduce the evaporation rate, since we imposed a dirt-dependent saturation vapour density at the evaporating interface. We also saw that, in the limit of slow suspended dirt diffusion, the transport of the dirt away from the evaporating interface limits the evaporation rate. The thickness, R of the deposited dirt layer was seen to vary spatially within the porous material. For slow deposition rates κ, R increased monotonically into the porous material, with the majority of the dirt concentrated at the end of the porous material. Conversely, for large κ, we observed an internal peak in R a short $O(1/\sqrt{\kappa})$ distance from the external surface of the material, and a uniform-thickness deposit through the majority of the remaining material. These spatial non-uniformities in R were shown to result in two distinct clogging mechanisms, in distinct regions of parameter space. The first clogging mechanism was dry-clogging, where deposition is slow, and suspended dirt is pushed further and further into the material as the evaporation front passes through the domain, until there is insufficient space for it all to deposit and the system clogs. A negligibly small amount of liquid is trapped in the system during dry clogging. By contrast, we found that wet clogging, defined as clogging when both liquid and suspended dirt are trapped in the porous material, occurs at sufficiently high dirt deposition rates κ and sufficiently slow suspended dirt diffusion rates σ^{-1}, such that the internal peak in R is too high, and the deposited dirt layer clogs the pore-space. We constructed a simplified paradigm model in the large κ situation, which captured the key

mechanisms of coupled accumulation, diffusion and deposition of dirt in a boundary layer at the evaporating interface, and derived a wet-clogging criterion.

For industrial drying scenarios, it may be important to control the dirt deposition profile. In particular it may be important to obtain as uniform a deposited layer through the material as possible, for instance if it is a dye or ink pigment that is being deposited. In the drying of filters and textiles after cleaning, clogging of the system should be avoided as much as possible, since a clogged filter can no longer perform its function. The drying rate might more easily be controlled than the diffusivity or deposition rate of the dirt (perhaps by controlling the ambient temperature or humidity) in order to avoid clogging-prone parameter regimes. Specifically, so long as the total initial amount of dirt is sufficiently low that wet-clogging will not occur, the drying rate should be kept slow (ie: κ should be made large), in order to avoid dry clogging.

For our numerical simulations, we chose a simple linear dependence of the saturation vapour density on the suspended dirt volume fraction $f(\theta) = 1 - \theta$, but this should be investigated further, since it is a key mechanism by which the accumulation of suspended dirt affects the evaporation rate. We have also focused the majority of our analysis in the case of $\alpha = 0$ so that the ambient humidity is very low, and the case $\beta = 0$, so that the dirt cannot re-suspend into the liquid once deposited. The effect of non-zero α and β should be further investigated. In particular, we would expect dry-clogging to be more prominent in the case $\beta > 0$, even for high deposition rates κ, since the suspended dirt volume fraction would not decay to zero ahead of the evaporation front in this case. We also used a two-dimensional microstructure, with circular solid inclusions. Three dimensional microstructures should be investigated, such as an array of spheres, which would result in different functional forms for C, ϕ and $\mathcal{D}$. In particular, the liquid region would remain connected when the dirt layers growing on neighbouring spheres met, although continuing growth of the dirt would eventually result in clogging in a similar way to our two-dimensional case. We expect qualitatively similar behaviour for alternative micro-geometries to our two-dimensional circles, including the possibility of both dry- and wet-clogging in the appropriate parameter regimes. The model and homogenisation analysis could be extended to other geometries, such as hexagonally packed cylinders, or square solid inclusions, as well as more general pore-scale geometries by using a level-set description of the microscale dirt–liquid interface, as in, for instance, Richardson & Chapman (2011). We should additionally investigate our model in higher macroscale dimensions, so that the evaporating interface is at $Y = H(X, T)$. In particular, in the slow-dirt-diffusion case $\sigma \gg 1$, which is analogous to a Stefan problem with constitutional supercooling, it is possible that the evaporating interface may become unstable.

A key assumption of our modelling was that the liquid remained stationary and did not flow. This resulted in a sharp evaporating interface separating the liquid/dirt and gas/vapour occupied regions of the porous material. In reality, a capillary-driven flow of liquid towards the surface of the porous material could draw suspended dirt to the surface as well, and we might anticipate even higher peaks in the deposited dirt layer thickness at or near the surface, increasing the likelihood of wet-clogging. Incorporating such capillary flows will be an important area for our future work.

The drying model derived in this paper captures many subtle couplings between the evaporation, accumulation, transport and deposition of dirt, and the transport of vapour out of the porous material during drying. The model itself and our subsequent analysis constitutes an important step towards an accurate prediction of deposited-dirt profiles and clogging behaviours, of particular relevance in the filtration and textile industry.

Acknowledgements. The authors thank U. Beuscher and V. Venkateshwaran (W.L. Gore & Associates,

Inc.), L. Hetherington (Defra), G. Anderson (Beko), and S. Tarkuç (Arçelik) for useful discussions. For the purpose of open access, the author has applied a Creative Commons Attribution (CC BY) licence to any Author Accepted Manuscript version arising from this submission.

Funding. E.K.L. is grateful for funding from the Industrial Fund of the Centre For Doctoral Training in Industrially Focused Mathematical Modelling. I.M.G. is grateful to the Royal Society for funding through a University Research Fellowship.

Declaration of Interests. The authors report no conflict of interest.

Data Availability. In compliance with both the University of Warwick and the University of Oxford's open access initiatives, the data in this paper is available from http://dx.doi.org/10.5281/zenodo.10932659.

Appendix A. Overview of homogenisation analysis

In this appendix we give an overview of the homogenisation analysis for the model (2.18), which holds within the pore-space, by which we obtain the effective model (2.20), that holds over the much simpler macroscale domain. We introduce macroscale space and time variables

$$T = \epsilon t, \qquad \boldsymbol{X} = \epsilon \boldsymbol{x}, \tag{A 1}$$

and denote the average position of the evaporating interface to be at $Y = H(T)$, which we assume is independent of X, so that the evaporating interface is flat and parallel to the surface of the porous material. Homogenisation of the partial differential equations (PDEs) describing Stokes flow of the gas mixture and advection–diffusion of both the vapour and the suspended dirt is fairly standard, and will follow, for instance Dalwadi *et al.* (2015). In order to derive effective boundary conditions for the motion of the evaporating interface on the macroscale, we follow the framework of Luckins *et al.* (2023), who study the motion of an evaporation front in porous media without dirt in the liquid. In terms of the macroscale spatial variables, we therefore consider a pore-scale ($O(\epsilon)$) boundary layer on either side of the evaporating interface $Y = H(T)$ in which the evaporating interface $y = h(x,t)$ moves on the microscale, as illustrated in the schematic in figure 15 and denoted as "inner" regions. The approach involves a coupled boundary layer analysis and homogenisation, alongside a more standard homogenisation to derive the effective PDEs in the "outer" regions (far from the evaporating interface) and careful matching between the inner and outer regions in order to derive the effective boundary conditions.

Since the analysis closely follows that of Luckins *et al.* (2023), we do not give all the details here. Instead we give an overview, indicating where the analysis deviates from that in our previous work. We begin in section A.1 with the analysis of the gas and vapour in $Y < H(T)$, before considering the liquid and dirt problem in $Y > H(T)$ in section A.2, and state the resulting effective model on the macroscale in section 2.3.

A.1. *Homogenisation of the gas–vapour problem in $Y < H(T)$*

The microscale problem for the flow of the gas–vapour mixture and advective–diffusive transport of vapour in $y < h(x,t)$, namely (2.18*a*) with (2.18*c*), (2.18*e*)–(2.18*g*), (2.18*i*), and (2.18*j*), is almost identical to that considered by Luckins *et al.* (2023) in the case $\alpha \ll 1$ (in their notation) for the chemistry boundary condition (2.18*i*). The differences are as follows:

(i) The chemistry interface condition (2.18*i*) is a Dirichlet condition for ρ that now depends on θ, and may vary in time and along the interface.

(ii) The microstructure of the porous material is no longer periodic: there may be spatial variation in the microstructure due to the dirt that has been deposited on the pore walls at earlier times. This will affect the flow and transport of vapour.

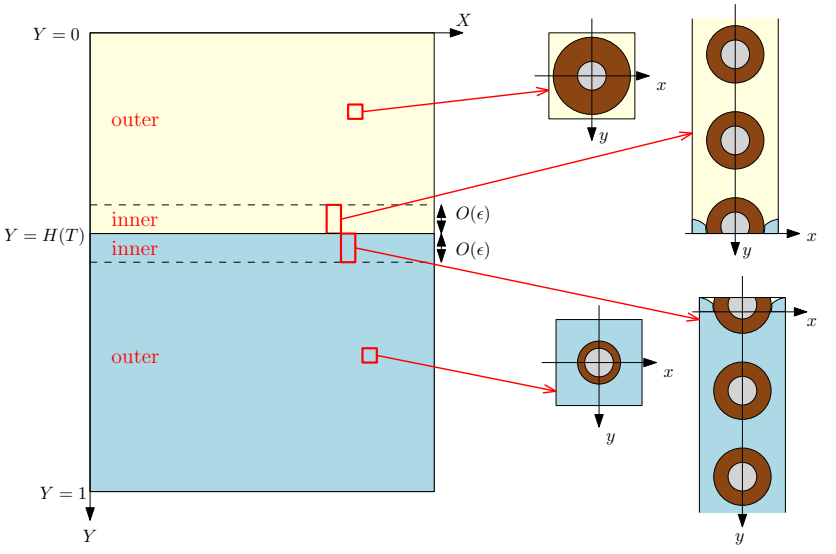

Figure 15: Schematic illustrating the homogenisation and boundary layer analysis. The solid microstructure of the porous material is shown by the grey circles in the insets, the gas–vapour mixture is shown in yellow and the dirt–liquid mixture in blue. The brown regions denote the layer of deposited dirt that is built up on the solid microstructure.

As discussed in section A.2 below, taking $\sigma = O(1)$ relative to ϵ means that θ is independent of the microscale space and time variables. This is important to our resolution of both points (i) and (ii) above. Specifically, since θ is independent of the microscale, the Dirichlet condition (2.18*i*) for ρ at the evaporating interface is independent of the microscale, and so our analysis in Luckins *et al.* (2023) follows as before. Furthermore, since θ only varies over the macroscale, we will see below that the thickness, R, of the deposited dirt layer on the pore microstructure only varies on the macroscale, and thus the porosity ϕ and effective diffusivity $\mathcal{D}$ in the region $y < h(x,t)$, occupied by the gas mixture, may only vary over a macro-lengthscale. The effect of a spatially varying porosity on the flow and advection of a fluid through porous media has been studied in, for instance, Dalwadi *et al.* (2015). Following Dalwadi *et al.* (2015), we may incorporate a spatially varying microstructure into the governing macroscale PDE for ρ. We also note that the derivation of the effective boundary conditions for the gas–vapour problem are unchanged from that of Luckins *et al.* (2023) by the spatially varying microstructure. This is because the variation of R on the macroscale only enters the equations at $O(\epsilon^2)$, whereas we only need to consider terms up to $O(\epsilon)$ in the inner region for the derivation of the interface conditions.

Adapting the analysis of Luckins *et al.* (2023) to include the spatial variation in R, we obtain at leading order the effective model, for $Y < H(T)$,

$$q_Y = 0, \qquad q = -kP_Y, \qquad \delta\phi\rho_T + \nu q\rho_Y = (\mathcal{D}\rho_Y)_Y\,, \tag{A 2}$$

with the (microscale-)time-averaged Darcy velocity, q, and pressure P given, respectively, by

$$q = H_T \int_{t=0}^{1/H_T} \iint_{\omega_f(R)} \boldsymbol{u}^{(0)}\,\mathrm{d}x\mathrm{d}y\,\mathrm{d}t, \qquad P = H_T \int_{t=0}^{1/H_T} p^{(0)}\,\mathrm{d}t, \tag{A 3}$$

where $\omega_f(R)$ is the pore-space domain (occupied by either the gas–vapour or liquid–dirt mixture). The micro-time averages are needed here since there may be fast oscillations in

the pressure and flow as the evaporating interface moves through the micro-scale cell. The effective diffusivity is defined to be

$$\mathcal{D} = \mathcal{D}(R) = \iint_{\omega_f(R)} 1 + W_y \,\mathrm{d}x\mathrm{d}y \tag{A 4}$$

where W is the solution of the cell problem given in Appendix B (which depends on the microscale geometry). We note that the permeability k, defined in Luckins *et al.* (2023), is also now a function of R (although we will not need this: in our macroscale geometry which we assume to be one-dimensional — with no variation in X — we will not need to solve for the average pressure P).

The interface conditions for q and ρ at $Y = H(T)$ are

$$q = -(1 - \delta\nu^{-1})\mathcal{F}H_T, \qquad \mathcal{D}\rho_Y = (1 - \nu\rho)\mathcal{F}H_T, \qquad \rho = f(\theta), \tag{A 5}$$

where $\mathcal{F}$, arising because of the averaging, is the total flux of liquid/vapour through the microscale evaporating interface in one micro-time-period. We will specify the value of $\mathcal{F}$ in (A 17) later. Finally, at the surface of the porous material, we have

$$\rho = \alpha, \quad P = 0, \qquad \text{at } Y = 0. \tag{A 6}$$

We note that (A 2), (A 5) and (A 6) may be combined, reducing the effective gas–vapour problem simply to a problem for ρ.

A.2. *Homogenisation of the liquid–dirt problem in $Y > H(T)$*

While the gas and vapour problem in section A.1 did not rely on any particular microscale geometry, for simplicity it is helpful to specify the porescale geometry when considering the dirt–liquid problem. As illustrated in figure 15, we assume that the porous structure is made from circular solid inclusions of dimensionless radius r_0, with a layer of dirt outside this, of dimensionless thickness $R \geqslant 0$. Thus the deposited-dirt–liquid interface, $\partial\omega_s(R)$, is at $|\boldsymbol{x}| = r_0 + R$, and the normal velocity of the interface is

$$V_n = R_t. \tag{A 7}$$

The microscale problem for θ, namely (2.18*b*), (2.18*d*), and (2.18*h*) is

$$\epsilon\sigma\theta_t = \nabla^2\theta \qquad \text{for } y < h(x,t), \tag{A 8}$$

$$\epsilon\sigma\theta\frac{h_t}{\sqrt{1+h_x^2}} + \nabla\theta\cdot\boldsymbol{m} = 0 \qquad \text{on } y = h(x,t), \tag{A 9}$$

$$\nabla\theta\cdot\boldsymbol{n}_s = \epsilon\sigma(\theta_* - \theta)R_t \qquad \text{on } \partial\omega_s, \tag{A 10}$$

$$R_t = \epsilon\kappa(\theta - \beta\chi_R) \qquad \text{on } \partial\omega_s, \tag{A 11}$$

where χ_R is an indicator function, with $\chi_R = 1$ if $R > 0$ and $\chi_R = 0$ if $R = 0$.

We homogenise these equations in the outer region (away from $Y = H(T)$ in a similar way to the filtration model of Dalwadi *et al.* (2015), or the reactive decontamination model of Luckins *et al.* (2020). The one difference is handling the multiple timescales, t and T, but this is dealt with straightforwardly as in Luckins *et al.* (2023). In particular, to leading order, we find that the suspended dirt volume fraction is independent of the microscale, so that diffusion is quasi-steady on the microscale, which is a direct result of our assumption that $\sigma = O(1)$. If, instead, $\sigma = O(\epsilon^{-1})$, then further analysis would be needed, since the suspended dirt would accumulate in a spatially non-uniform manner within the periodic cell.

The resulting effective equations for the suspended dirt volume fraction, θ, and the

deposited dirt layer thickness, R, in $H(T) < Y < 1$ are

$$\sigma\phi\theta_T = (\mathcal{D}\theta_Y)_Y - \sigma\kappa C(\theta_* - \theta)(\theta - \beta\chi_R), \tag{A 12}$$

$$R_T = \kappa(\theta - \beta\chi_R), \tag{A 13}$$

where $\phi(R) = 1 - \pi(r_0 + R)^2$ is the local porosity, $\mathcal{D}(R)$ is the local effective diffusivity (defined in (A 4)), and $C(R) = 2\pi(r_0 + R)$ is the circumference (or surface area) of the deposited dirt layer. Although (A 13) is an ODE for R in time T, R may vary spatially, since the dirt-deposition rate depends on the local suspended dirt volume fraction θ.

At the edge of the macroscale domain, $Y = 1$, the macroscale version of (2.18*k*) holds and so we have

$$\theta_Y = 0 \qquad \text{on } Y = 1. \tag{A 14}$$

Following the same boundary layer analysis for the inner region as in the gas–vapour problem in Luckins *et al.* (2023), we obtain a macroscale boundary condition for θ at $Y = H(T)$, namely

$$\sigma\mathcal{F}H_T\theta + \mathcal{D}\theta_Y = 0 \qquad \text{on } Y = H(T). \tag{A 15}$$

By considering the overall conservation of dirt, we now show that $\mathcal{F}$ (the total flux of liquid through the microscale evaporating interface in one micro-time-period) must be exactly the porosity, ϕ, at $Y = H(T)$. Integrating the suspended dirt conservation equation (A 12) over the macroscale domain $Y \in [H, 1]$, and using Leibniz' rule, the boundary conditions (A 14)–(A 15), the equation (A 13) for R_T, and using the fact that $\phi_T = -CR_T$ by definition, we obtain

$$\frac{\mathrm{d}}{\mathrm{d}T}\left(\int_{H(T)}^{1} \phi\theta \,\mathrm{d}Y\right) = H_T\theta|_{Y=H}\,(\mathcal{F} - \phi|_{Y=H}) - \int_{H(T)}^{1} R_T C\theta_* \,\mathrm{d}Y. \tag{A 16}$$

We can interpret this as the overall conservation of suspended dirt: on the left is the rate of change of total amount of dirt suspended in the liquid, and the final term on the right is the rate at which suspended dirt is "lost" to the deposited layer on the solid. There is no other way that dirt should be lost or gained, and so the additional term (the first term on the left) must equal zero. Thus we require

$$\mathcal{F} = \phi|_{Y=H}. \tag{A 17}$$

In Luckins *et al.* (2023), for a pure evaporation problem with no dirt in the evaporating liquid, it was argued that $\mathcal{F} = \phi|_{Y=H}$ by consideration of the microscale conservation of mass of liquid: all the liquid occupying the unit cell (ϕ) had to pass through the evaporating interface as vapour ($\mathcal{F}$) in order for the interface to move down through the cell. It may therefore seem counter-intuitive that $\mathcal{F} = \phi|_{Y=H}$ when there is suspended dirt in the liquid also. However, since we assume $\sigma = O(1)$ and so dirt diffusion is quasi-steady on the microscale, all the suspended dirt contained within the unit cell is forced out by diffusion in order that the evaporating interface can pass through the cell. Thus the full volume ϕ of liquid passes through the interface in one time-period, in keeping with $\mathcal{F} = \phi|_{Y=H}$.

Appendix B. The cell problem for the effective diffusivity $\mathcal{D}$

As shown by Luckins *et al.* (2023), the effective diffusivity $\mathcal{D}(R)$ given by (A 4) may be found by solving a cell problem for W, namely

$$\nabla^2 W = 0 \qquad \text{for } x, y \in \omega_f(R), \tag{B 1}$$

$$(\nabla W + \boldsymbol{e}_1)\cdot\boldsymbol{n} = 0 \qquad \text{on } |\boldsymbol{x}| = r_0 + R, \tag{B 2}$$

$$W \text{ periodic in both } x \text{ and } y \qquad \text{over } \omega(R), \tag{B 3}$$

where $\boldsymbol{n}$ is the unit normal to the solid-liquid interface at $|\boldsymbol{x}| = r_0 + R$. The definition of the effective diffusivity $\mathcal{D}$ presented in (A 4) is common to many diffusion problems in multi-scale geometries. The solution $\mathcal{D}$ has been computed for our circular geometry by, for instance Bruna & Chapman (2015) and Dalwadi *et al.* (2015). We use the numerically computed solution of Dalwadi *et al.* (2015) in the numerical simulations in this paper.

REFERENCES

Abney, S.E., Ijaz, M.K., McKinney, J. & Gerba, C.P. 2021 Laundry hygiene and odor control: state of the science. *Applied and Environmental Microbiology* **87** (14), e03002–20.

Breward, C., Brosa Planella, F., Edwards, D.A., Kiradjiev, K., Kovacs, A., Llewellyn Smith, S., Rumschitzki, D., Sanaei, P., Sun, Y., Witelski, T., Zyskin, M., Tilley, B., Broadbridge, P., Gu, B., Adriazola, J., Barra, V., Fok, P.-W., Ockendon, H. & Ockendon, J. 2020 Pore-level analysis in "Evaporation from porous media'. 36th MPI Workshop report, University of Vermont, https://mpi2020.w3.uvm.edu/finalReports/FinalReport_Gore_2020.pdf.

Bruna, M. & Chapman, S.J. 2015 Diffusion in spatially varying porous media. *SIAM Journal on Applied Mathematics* **75** (4), 1648–1674.

Cussler, E. L. 2009 *Diffusion: mass transfer in fluid systems (3rd ed.)*. Cambridge University Press, Cambridge, UK.

Dalwadi, M.P., Griffiths, I.M. & Bruna, M. 2015 Understanding how porosity gradients can make a better filter using homogenization theory. *Proceedings of the Royal Society A: Mathematical, Physical and Engineering Sciences* **471** (2182), 20150464.

D'Ambrosio, H.-M., Colosimo, T., Duffy, B.R., Wilson, S.K., Yang, L., Bain, C.D. & Walker, D.E. 2021 Evaporation of a thin droplet in a shallow well: theory and experiment. *Journal of Fluid Mechanics* **927**, A43.

Deegan, R.D., Bakajin, O., Dupont, T.F., Huber, G., Nagel, S.R. & Witten, T.A. 1997 Capillary flow as the cause of ring stains from dried liquid drops. *Nature* **389** (6653), 827–829.

Deegan, R.D., Bakajin, O., Dupont, T.F., Huber, G., Nagel, S.R. & Witten, T.A. 2000 Contact line deposits in an evaporating drop. *Physical Review E* **62** (1), 756.

Dressaire, E. & Sauret, A. 2017 Clogging of microfluidic systems. *Soft Matter* **13** (1), 37–48.

Epstein, N. 1988 Particulate fouling of heat transfer surfaces: mechanisms and models. In *Fouling Science and Technology*, pp. 143–164. Springer.

Fei, L., Qin, F., Zhao, J., Derome, D. & Carmeliet, J. 2022 Pore-scale study on convective drying of porous media. *Langmuir* **38(19)**, 6023–6035.

Flury, M. & Aramrak, S. 2017 Role of air-water interfaces in colloid transport in porous media: A review. *Water Resources Research* **53** (7), 5247–5275.

Geng, Y., Kamilova, A.A. & Luckins, E.K. 2023 Fluid-flow effects in the reactive decontamination of porous materials driven by chemical swelling or contraction. *Journal of Engineering Mathematics* **141** (1), 11.

Gudipaty, T., Stamm, M.T., Cheung, L.S.L., Jiang, L. & Zohar, Y. 2011 Cluster formation and growth in microchannel flow of dilute particle suspensions. *Microfluidics and Nanofluidics* **10**, 661–669.

Ji, H. & Sanaei, P. 2023 Mathematical model for filtration and drying in filter membranes. *Physical Review Fluids* **8** (6), 064302.

Kaplan, C.N. & Mahadevan, L. 2015 Evaporation-driven ring and film deposition from colloidal droplets. *Journal of Fluid Mechanics* **781**, R2.

Karapetsas, G., Sahu, K.C. & Matar, O.K. 2016 Evaporation of sessile droplets laden with particles and insoluble surfactants. *Langmuir* **32** (27), 6871–6881.

Lehmann, P., Assouline, S. & Or, D. 2008 Characteristic lengths affecting evaporative drying of porous media. *Physical Review E* **77** (5), 056309.

Linkhorst, J., Beckmann, T., Go, D., Kuehne, A.J.C. & Wessling, M. 2016 Microfluidic colloid filtration. *Scientific Reports* **6** (1), 22376.

Luckins, E.K., Breward, C.J.W., Griffiths, I.M. & Please, C.P. 2023 A homogenised model for the motion of evaporating fronts in porous media. *European Journal of Applied Mathematics* pp. 1–32, doi:10.1017/S0956792522000419.

Luckins, E., Breward, C.J.W., Griffiths, I.M. & Wilmott, Z. 2020 Homogenisation problems in reactive decontamination. *European Journal of Applied Mathematics* **31** (5), 782–805.

Mampallil, D. & Eral, H.B. 2018 A review on suppression and utilization of the coffee-ring effect. *Advances in Colloid and Interface Science* **252**, 38–54.

Moore, M.R., Vella, D. & Oliver, J.M. 2021 The nascent coffee ring: how solute diffusion counters advection. *Journal of Fluid Mechanics* **920**, A54.

Murisic, N. & Kondic, L. 2011 On evaporation of sessile drops with moving contact lines. *Journal of Fluid Mechanics* **679**, 219–246.

Nowicki, S.C., Davis, H.T. & Scriven, L.E. 1992 Microscopic determination of transport parameters in drying porous media. *Drying Technology* **10** (4), 925–946.

Or, D., Lehmann, P., Shahraeeni, E. & Shokri, N. 2013 Advances in soil evaporation physics – a review. *Vadose Zone Journal* **12** (4), 1–16.

Pel, L., Landman, K.A. & Kaasschieter, E.F. 2002 Analytic solution for the non-linear drying problem. *International Journal of Heat and Mass Transfer* **45** (15), 3173–3180.

Popov, Y.O. 2005 Evaporative deposition patterns: spatial dimensions of the deposit. *Physical Review E* **71** (3), 036313.

Richardson, G. & Chapman, S.J. 2011 Derivation of the bidomain equations for a beating heart with a general microstructure. *SIAM Journal on Applied Mathematics* **71** (3), 657–675.

Sanaei, P., Breward, C.J.W., Ellis, M.A., Han, S., Holzer, B., Ji, H., El Kahza, H., Llewellyn Smith, S.G., Parsa, S., Reynolds, H., Troy, J., Witelski, T., Zhang, N. & Zyskin, M. 2022 Evaporation and deposition in porous media. Mathematics in Industry Reports, Cambridge Open Engage, doi:10.33774/miir-2022-wq8fl.

Shampine, L.F. & Reichelt, M.W. 1997 The MATLAB ODE suite. *SIAM J. Sci. Comput.* **18** (1), 1–22.

Shokri, N., Lehmann, P. & Or, D. 2008 Effects of hydrophobic layers on evaporation from porous media. *Geophysical Research Letters* **35** (19).

Soltman, D. & Subramanian, V. 2008 Inkjet-printed line morphologies and temperature control of the coffee ring effect. *Langmuir* **24** (5), 2224–2231.

Stamm, M.T., Gudipaty, T., Rush, C., Jiang, L. & Zohar, Y. 2011 Particle aggregation rate in a microchannel due to a dilute suspension flow. *Microfluidics and Nanofluidics* **11**, 395–403.

Tsimpanogiannis, I.N., Yortsos, Y.C., Poulou, S., Kanellopoulos, N. & Stubos, A.K. 1999 Scaling theory of drying in porous media. *Physical Review E* **59** (4), 4353.

Vu, H T & Tsotsas, E 2018 Mass and heat transport models for analysis of the drying process in porous media: a review and numerical implementation. *International Journal of Chemical Engineering* **2018**.

Whitaker, S. 1977 Simultaneous heat, mass, and momentum transfer in porous media: a theory of drying. In *Advances in Heat Transfer*, , vol. 13, pp. 119–203. Elsevier.

Wilson, S.K. & D'Ambrosio, H.-M. 2023 Evaporation of sessile droplets. *Annual Review of Fluid Mechanics* **55**, 481–509.

Zamani, A. & Maini, B. 2009 Flow of dispersed particles through porous media —– deep bed filtration. *Journal of Petroleum Science and Engineering* **69** (1-2), 71–88.